Data in Brief 37 (2021) 107190

Contents lists available at ScienceDirect

Data in Brief

journal homepage: www.elsevier.com/locate/dib

Data Article

Dataset for the synthesis and application of single-component heterogeneous catalysts based on zinc and tin for the cycloaddition of pure, diluted, and impure CO_2 to epoxides under mild conditions

Chalida Phungpanya[a], Ounjit Sodpiban[a], Silvano Del Gobbo[a], Sunatda Arayachukiat[b], Taradon Piromchart[b], Valerio D'Elia[a,*]

[a] *Department of Material Science and Engineering, School of Molecular Science and Engineering, Vidyasirimedhi Institute of Science and Technology (VISTEC), 21210, Payupnai, WangChan, Rayong, Thailand*
[b] *PTT Exploration and Production Company Limited, Energy Complex Building A, Floors 6, 19 – 36, 555/1 Vibhavadi Rangsit Road, Chatuchak, Bangkok 10900, Thailand*

ARTICLE INFO

Article history:
Received 28 April 2021
Revised 19 May 2021
Accepted 27 May 2021
Available online 1 June 2021

Keywords:
Heterogeneous Catalyst
Synthesis
Silica
Metal halide grafting
Ionic liquid grafting
Zinc
Tin
CO_2 conversion
Cyclic carbonates

ABSTRACT

The cycloaddition of CO_2 to epoxides under mild conditions is a growing field of research and a viable strategy to recycle CO_2 in the form of cyclic carbonates as useful intermediates, solvents, and additives. This target requires readily accessible and recyclable catalysts whose synthesis does not involve expensive monomers, multistep procedures, coupling reagents, etc. Additionally, the catalysts should be active under atmospheric pressure and tolerate impurities such as methane and H_2S. In a recent manuscript (**Rational engineering of single-component heterogeneous catalysts based on abundant metal centers for the mild conversion of pure and impure CO_2 to cyclic carbonates;** *Chemical Engineering Journal* 422 (2021) 129930) we have developed strategies to prepare efficient heterogeneous catalysts for the cycloaddition reaction of CO_2 to epoxides. Such materials consist of dispersions of metal halides ($ZnCl_2$ or $SnCl_4$) on silica support that is further functionalized with ionic liquids bearing nucle-

DOI of original article: 10.1016/j.cej.2021.129930
* Corresponding author.
E-mail address: valerio.delia@vistec.ac.th (V. D'Elia).

https://doi.org/10.1016/j.dib.2021.107190
2352-3409/© 2021 The Author(s). Published by Elsevier Inc. This is an open access article under the CC BY-NC-ND license (http://creativecommons.org/licenses/by-nc-nd/4.0/)

ophilic halide moieties for cooperative epoxide activation and ring-opening. Herein, we provide useful complementary data for the characterization of the prepared materials in the form of: SEM images of materials (SEM: scanning electron microscope), SEM-EDS images of materials (EDS: Energy-dispersive X-ray spectroscopy), TEM images of materials (TEM: transmission electron microscope); XPS (X-ray photoelectron spectroscopy) survey spectra of most active catalysts and related high-resolution spectra in spectral regions of interest, BET (Brunauer–Emmett–Teller) physisorption isotherms of materials, raw ^{1}H NMR spectra of catalytic reactions to verify the reproducibility of the reaction outcome and identify the reaction products.

© 2021 The Author(s). Published by Elsevier Inc.
This is an open access article under the CC BY-NC-ND license (http://creativecommons.org/licenses/by-nc-nd/4.0/)

Specifications Table

Subject	Chemical Engineering: Catalysis
Specific subject area	Inorganic Chemistry and Physical Characterization
Type of data	Table Image Figure
How data were acquired	SEM/EDS mappings were acquired on a JEOL JSM-7610F field emission scanning electron microscope equipped with an Oxford Instruments X-Max150 EDS. TEM images were acquired on a JEOL JEM-ARM 200F electron microscope equipped with Energy dispersive X-ray analyser (EDS) JEOL EX-37001. Images acquired by TEM Center Ver. 2.0.15.6527 and analysed by Gatan Digital Micrograph Ver. 3.22.1461.0 XPS survey spectra and high-resolution spectra were acquired on a JEOL JPS-9010MC spectrometer with SpectraSurf Ver. 1.9.3 acquisition and analysis software. BET physisorption isotherms were acquired on a BELSORP-Mini II analyser with BELSORP-mini Ver. 2.5.10 measuring software and BELMaster™ Version 6.3.2.1 analysing software ^{1}H NMR spectra were acquired on a Bruker Avance III 600 MHz with Topspin 3.6.2 software
Data format	Raw Analyzed
Parameters for data collection	SEM/EDS – High resolution SEM mode; 1 kV electron acceleration, 11-1 mA filament current. EDS mode; 15 kV electron acceleration, 7-8 mA filament current. Chamber pressure = $2.0{\cdot}10^{-5}$ Pa TEM – High resolution mode; 200 kV electron acceleration, 11-1 μA filament current. Chamber pressure = $2.0{\cdot}10^{-5}$ Pa XPS – Mg Kα source (1253.6 eV) working at 12 kV and 25 mA. Chamber pressure = 10^{-8} Pa, temperature = 25°C. Energy pass = 50 eV, binding energy range = 0-1100 eV, steps = 1 eV BET – Measurement by N_2 adsorption/desorption at -196°C NMR – 600 MHz Avance III NMR spectrometer operating at 25°C with 5 mm TCI CryoProbe Prodigy and z-gradients ^{1}H frequency = 600.13 MHz
Description of data collection	SEM/EDS – Finely dispersed catalyst powders were deposited on carbon tape glued to Al stubs in a N_2-filled glove box and transferred to the XPS instrument by a sealed sample holder for air sensitive samples. TEM – Catalyst powders were dispersed in dry dichloromethane and deposited by dipping on Cu TEM grids. Coated grids were kept under N_2

(*continued on next page*)

	before plasma treated and loaded in the TEM pre-chamber. XPS – samples in the form of powder were deposited on carbon tape glued to the sample holder in a N_2 filled glove box and transferred to the XPS instrument by a sealed manipulator for air sensitive samples. BET – Catalyst powders were filled to the sample tubes and pretreated at 100°C for 16 h under 10^{-2} kPa vacuum before measurement. NMR – All compounds were measured in $CDCl_3$ at room temperature by adding a drop of crude reaction mixture to 0.7 mL $CDCl_3$ in a standard NMR tube.
Data source location	Vidyasirimedhi Institute of Science and Technology (VISTEC), department of materials science engineering, school of molecular science engineering, 555 Moo 1, 21210, Payupnai, WangChan, Rayong, Thailand. (13.002395649932376, 101.44350075242147).
Data accessibility	https://data.mendeley.com/datasets/dx5zpgmwp6/3 (https://doi.org/10.17632/dx5zpgmwp6.3)
Related research article	O. Sodpiban, C. Phungpanya, S. Del Gobbo,* S. Arayachukiat, T. Piromchart and V. D'Elia* Rational engineering of single-component heterogeneous catalysts based on abundant metal centers for the mild conversion of pure and impure CO_2 to cyclic carbonates Chemical Engineering Journal 422 (2021) 129930, DOI: 10.1016/j.cej.2021.129930

Value of the Data

- These data are important for the complete characterization (electron microscopy, XPS and BET isotherms) of efficient catalytic materials for the cycloaddition of CO_2 to epoxides under mild conditions and for assessing (^{1}H NMR of crude catalytic reactions) the reproducibility of the catalytic reactions using the most efficient catalysts among the synthesized materials.
- Researchers in materials science and catalysis can find the spectroscopic data, microscopic images, physicochemical characterization, and spectra of catalytic reactions helpful when characterizing comparable materials and applying them in catalytic cycloaddition reactions of epoxides.
- Reported data can be used for the design of new catalysts based on co-immobilized metal centres and ionic liquids and for the interpretation of crude spectra of catalytic cycloaddition reactions involving epoxides.

1. Data Description

The data in this article refer to the materials in Table 1 that were prepared as catalysts for the cycloaddition of CO_2 to epoxides [1-5] and that are described in detail (including the structure of ionic liquids **IL-I** and **IL-Br**) in *Rational engineering of single-component heterogeneous catalysts based on abundant metal centers for the mild conversion of pure and impure CO_2 to cyclic carbonates* [6].

The SEM and TEM images of the **tt-$SiO_{2\text{-}150}$** sample in Fig. 1 show the aggregated nature of the Aerosil fumed silica nanoparticles used as the support in this work and their morphology by using two different magnifications. The SEM images of **IL-I@SiO_2** and **IL-Br@SiO_2** in Fig. 2 show that the aggregated nature of the silica materials is preserved after grafting ionic liquids on the support. The SEM images of $ZnCl_2$-based catalysts in Fig. 3 and of $SnCl_4$-based catalysts in Fig. 4 show a clear effect of increasing metal and ionic liquid loadings on particles aggregation. The SEM-EDS images for $ZnCl_2$-based catalysts (Figs. 5-7) and $SnCl_4$-based catalysts (Figs. 8-10) show the uniform distribution of Zn, Cl, I elements (for $ZnCl_2$-based catalysts) and of Sn, Cl, Br elements (for Sn-based catalysts).

Table 1
List of materials mentioned in this article.

Material	Brief description
tt-$SiO_{2\text{-}150}$	Support
IL-I@SiO_2	Ionic liquid **IL-I** (iodide anion) grafted on support
IL-Br@SiO_2	Ionic liquid **IL-Br** (bromide anion) grafted on support
$ZnCl_2$(0.36)-IL-I	Catalytic material based on $ZnCl_2$ with **IL-I**
$ZnCl_2$-0.45@SiO_2	Precursor of **$ZnCl_2$(0.36)-IL-I** prior to **IL-I** grafting
$ZnCl_2$(1.99)-IL-I	Catalytic material based on $ZnCl_2$ with **IL-I**
$ZnCl_2$-2.26@SiO_2	Precursor of **$ZnCl_2$(1.99)-IL-I** prior to **IL-I** grafting
$ZnCl_2$(3.29)-IL-I	Catalytic material based on $ZnCl_2$ with **IL-I**
$ZnCl_2$-4.23@SiO_2	Precursor of **$ZnCl_2$(3.29)-IL-I** prior to **IL-I** grafting
$ZnCl_2$(5.62)-IL-I	Catalytic material based on $ZnCl_2$ with **IL-I**
$ZnCl_2$-7.89@SiO_2	Precursor of **$ZnCl_2$(5.62)-IL-I** prior to **IL-I** grafting
$SnCl_4$(0.24)-IL-Br	Catalytic material based on $SnCl_4$ with **IL-Br**
$SnCl_4$-0.32@SiO_2	Precursor of **$SnCl_4$(0.24)-IL-Br** prior to **IL-Br** grafting
$SnCl_4$(0.66)-IL-Br	Catalytic material based on $SnCl_4$ with **IL-Br**
$SnCl_4$-0.84@SiO_2	Precursor of **$SnCl_4$(0.66)-IL-Br** prior to **IL-Br** grafting
$SnCl_4$(1.06)-IL-Br	Catalytic material based on $SnCl_4$ with **IL-Br**
$SnCl_4$-1.45@SiO_2	Precursor of S**nCl_4(1.06)-IL-Br** prior to **IL-Br** grafting
$SnCl_4$(1.93)-IL-Br	Catalytic material based on $SnCl_4$ with **IL-Br**
$SnCl_4$-2.89@SiO_2	Precursor of **$SnCl_4$(1.93)-IL-Br** prior to **IL-Br** grafting

The survey XPS spectrum of **$ZnCl_2$-2.26@SiO_2** (Fig. 11) confirms the presence of relevant elements Zn and Cl from grafting of the $ZnCl_2$ precursor by ball milling. A high-resolution overview of all relevant spectral regions of this material (C 1s, O 1s, Zn 2p, Cl 2p, Si 2p) is provided in Fig. 12. The survey spectrum of **$SnCl_4$-0.84@SiO_2** (Fig. 13) shows the presence of tin and chlorine elements from the $SnCl_4$ precursor grafted by impregnation with the relevant spectral regions (C 1S, O 1s, Si 2p, Sn 3d and Cl 2p) being displayed in high-resolution in Fig. 14. The survey XPS spectrum of **$ZnCl_2$(1.99)-IL-I** (Fig. 15) shows the presence of Zn, Cl, N, I elements from $ZnCl_2$ and **IL-I** with the relevant spectral regions (C 1s, N 1s, O 1s, Si 2p, Cl 2p, I 3d and Zn 2p) being provided in high-resolution in Fig. 16. This is also the case of **$SnCl_4$(0.66)-IL-Br** (See Fig. 17 for survey spectrum, Fig. 18 for the high-resolution spectra in the C 1s, N 1s, O 1s, Si 2p, Cl 2p, Br 3d and Sn 3d regions) showing the presence of characteristic elements Sn, Cl (from $SnCl_4$) and N, Br from **IL-Br**. The XPS spectra in Figs. 19-22 refer to the spent materials **$ZnCl_2$(1.99)-IL-I** (Fig. 19 (survey), Fig. 20 (high-resolution in the C 1s, N 1s, O 1s, Si 2p, Cl 2p, I 3d and Zn 2p regions)) and **$SnCl_4$(0.66)-IL-Br** ((Fig. 21 (survey), Fig. 22 (high-resolution in the C 1s, N 1s, O 1s, Si 2p, Cl 2p, Br 3d and Sn 3d regions)) after five catalytic cycles with a CO_2 feed containing H_2S. These figures show the apparent absence of sulfur contaminant in the survey spectra and the presence of the same elements as in the pristine materials but with lower intensity in the case of halides (due to dehalogenation).

The BET adsorption/desorption isotherms in Fig. 23 are for the $ZnCl_2$-based catalytic materials and those in Fig. 24 for the $SnCl_4$-based catalytic materials. Such isotherms show the lack of porosity of these materials as expected given the non-porous nature of the support (See isotherm shown in Fig. 25 along with metal-free catalytic materials **IL-I@SiO_2** and **IL-Br@SiO_2**).

The ^{1}H NMR spectra of catalytic cycloaddition reactions carried out under different reaction conditions[6] in Figs. 26-63 generally show the formation of signals relative to the cyclic carbonate products in the 4-5 ppm region and the disappearance of the signals relative to the epoxide substrates in the 2-3 ppm region [7-9]. These data are useful to estimate the conversion of epoxides and to calculate conversion values based on the integration of corresponding signals of products and epoxides [10-12]. These data generally confirm the complete or nearly complete conversion of epoxide substrates and the absence of evident reaction by-products and the reproducible application of the catalysts

Supplementary material includes the raw data for XPS spectra, BET physisorption experiments and ^{1}H NMR experiments.

2. Experimental Design, Materials and Methods

The preparation of all compounds in Table 1 and the experimental procedure for catalytic reactions is described in Rational engineering of single-component heterogeneous catalysts based on abundant metal centers for the mild conversion of pure and impure CO_2 to cyclic carbonates [6].

2.1. Scanning electron microscopy (SEM)

SEM images of materials were acquired by a JEOL JSM-7610F field emission scanning electron microscope equipped with an Oxford Instruments X-Max150 EDS. Samples were prepared by tapping adhesive carbon stabs on paper smeared with the catalyst powders. No sputtering metallization was used.

2.2. Transmission electron microscopy (TEM)

TEM images were obtained on a JEOL JEM-ARM 200F electron microscope. All samples were dispersed in dry dichloromethane and coated by three dipping/drying cycles on TEM grids (Ted Pella Ultrathin C Type-A 400 mesh, Cu). All samples were plasma-treated before the insertion in the microscope vacuum pre-chamber.

2.3. X-ray photoelectron spectroscopy (XPS)

X-ray photoelectron spectroscopy (XPS) was performed by a JEOL JPS-9010MC spectrometer utilizing a Mg Kα source (1253.6 eV) working at 12 kV and 25 mA. All XPS spectra were acquired under high vacuum (10^{-8} Pa) at room temperature. All samples were prepared by compacting the catalysts powders on carbon tape (9×9 mm^2 area). The survey scans were acquired with a pass energy of 50 eV, a binding energy range of 0-1100 eV and steps of 1 eV. Spectral regions relative to specific elements of interest were acquired with high resolution by averaging over a large number of spectra in order to have a good signal to noise ratio. All binding energies were charge corrected by referencing to the carbon peak C 1s at 284.80 eV.

2.4. Brunauer-emmett-teller (BET) analysis

The surface areas of **tt-SiO$_{2\text{-}150}$** support and of powder catalysts were measured using a BELSORP-mini II instrument (BEL Japan) via N_2 adsorption/desorption isotherm at liquid nitrogen temperature (-196°C). Prior to the measurement, the samples were added to the sample tubes and subsequently pretreated under vacuum (at 100°C for 16 h) by a BELPREP-vac II instrument (MicrotracBEL) to remove undesired moisture adsorbed on the surface. The surface area was calculated by BET method using a linearity range of the relative pressure (P/P_0) = 0.05-0.35.

2.5. Nuclear magnetic resonance (NMR) spectroscopy

All NMR spectra of catalytic reactions were collected using a 600 MHz Bruker Avance III NMR spectrometer operating at 25°C with 5 mm TCI CryoProbe Prodigy and z-gradients. All chemical shifts (δ ppm) were referenced to the internal standard tetramethyl silane (TMS; ^{1}H resonances appear at 0.00 ppm) present in $CDCl_3$. ^{1}H frequency = 600.13 MHz. To collect the crude reaction spectra, an aliquot of the reaction product was withdrawn and added into an NMR tube containing 0.7 mL $CDCl_3$.

Electron microscopy images

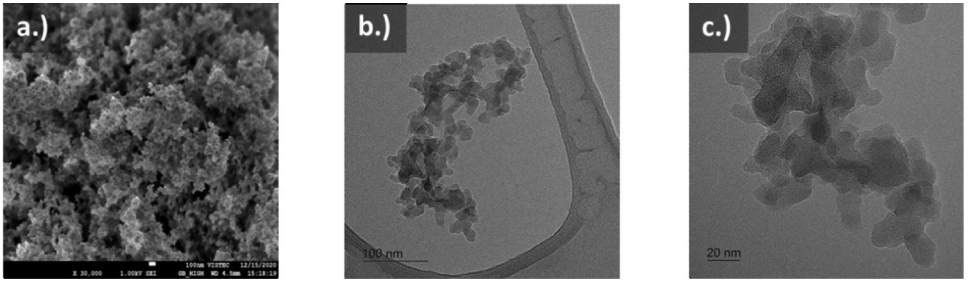

Fig. 1. a.) SEM image, **b.)** TEM image at 100k magnifications and **c.)** TEM image at 500k magnifications of **tt-$SiO_{2\text{-}150}$**.

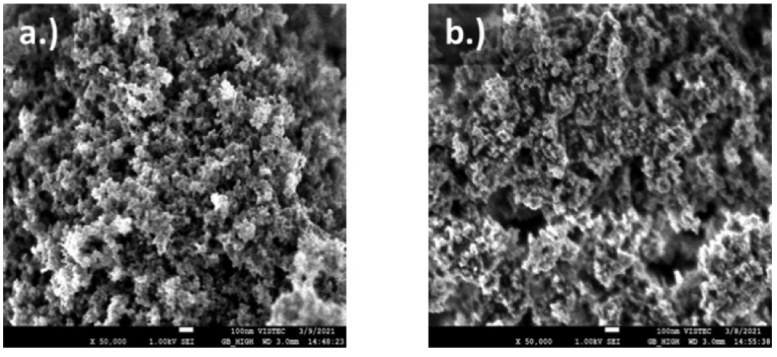

Fig. 2. SEM images of **a.) IL-I@SiO_2** and **b.) IL-Br@SiO_2**.

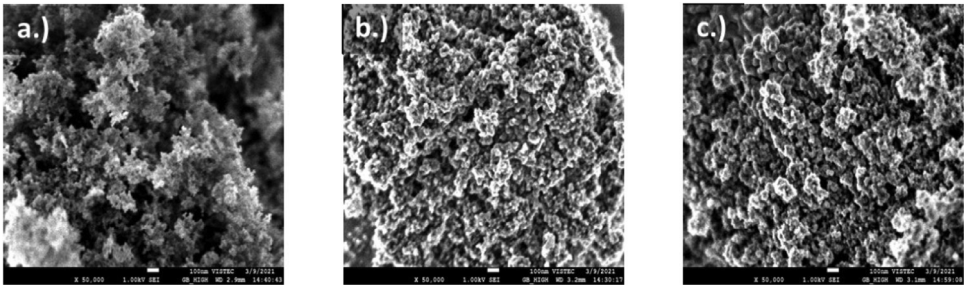

Fig. 3. SEM images of **a.) $ZnCl_2$(0.36)-IL-I, b.) $ZnCl_2$(3.29)-IL-I** and **c.) $ZnCl_2$(5.62)-IL-I**.

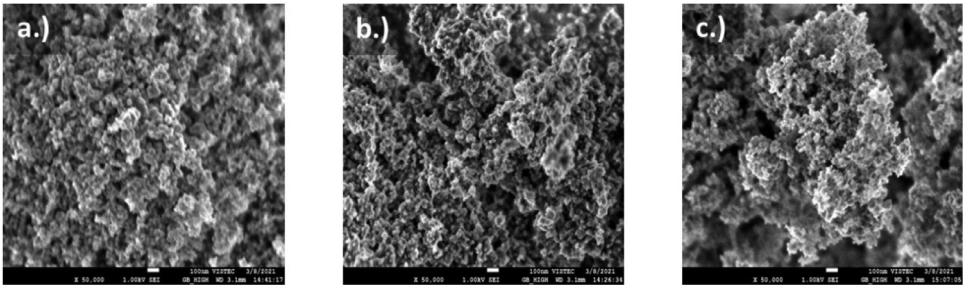

Fig. 4. SEM image of **a.)** **$SnCl_4$(0.24)-IL-Br**, **b.)** **$SnCl_4$(1.06)-IL-Br** and **c.)** **$SnCl_4$(1.93)-IL-Br**.

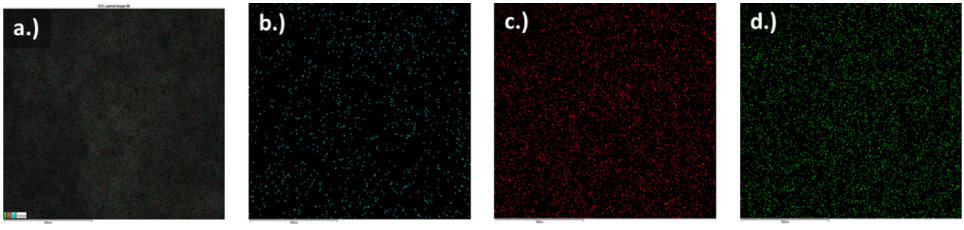

Fig. 5. **a.)** EDS mapping and **b-d.)** dispersion of Zn, Cl and I elements for **$ZnCl_2$(0.36)-IL-I**.

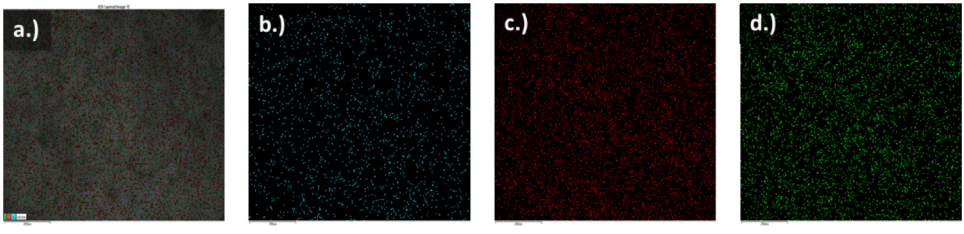

Fig. 6. **a.)** EDS mapping and **b-d.)** dispersion of Zn, Cl and I elements for **$ZnCl_2$(3.29)-IL-I**.

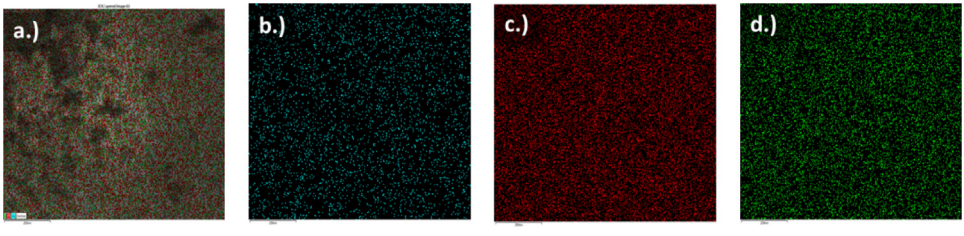

Fig. 7. **a.)** EDS mapping and **b-d.)** dispersion of Zn, Cl and I elements for **$ZnCl_2$(5.62)-IL-I**.

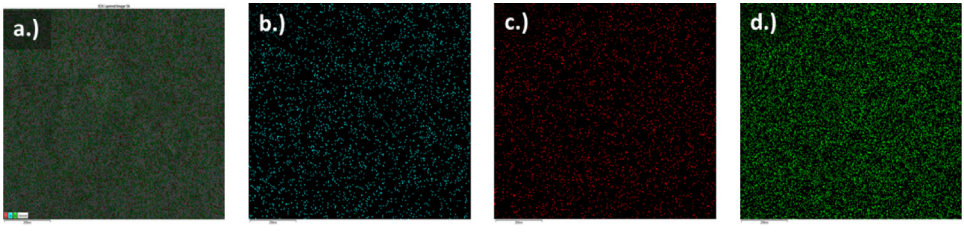

Fig. 8. **a.)** EDS mapping and **b-d.)** dispersion of Sn, Cl and Br elements for **$SnCl_4$(0.24)-IL-Br**.

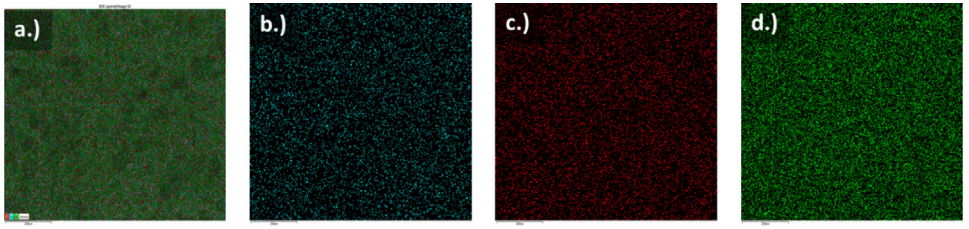

Fig. 9. a.) EDS mapping and **b-d.)** dispersion of Sn, Cl and Br elements for **$SnCl_4$(1.06)-IL-Br**.

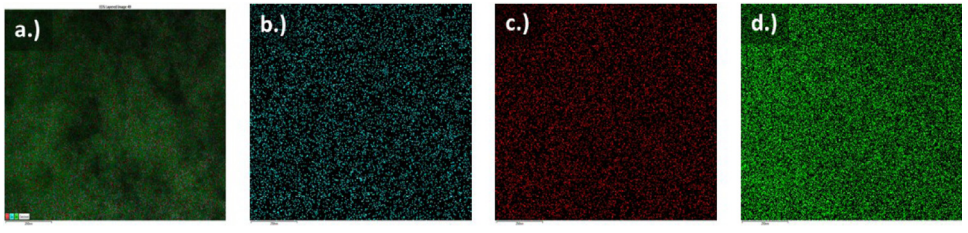

Fig. 10. a.) EDS mapping and **b-d.)** dispersion of Sn, Cl and Br elements for **$SnCl_4$(1.93)-IL-Br**.

XPS Spectra

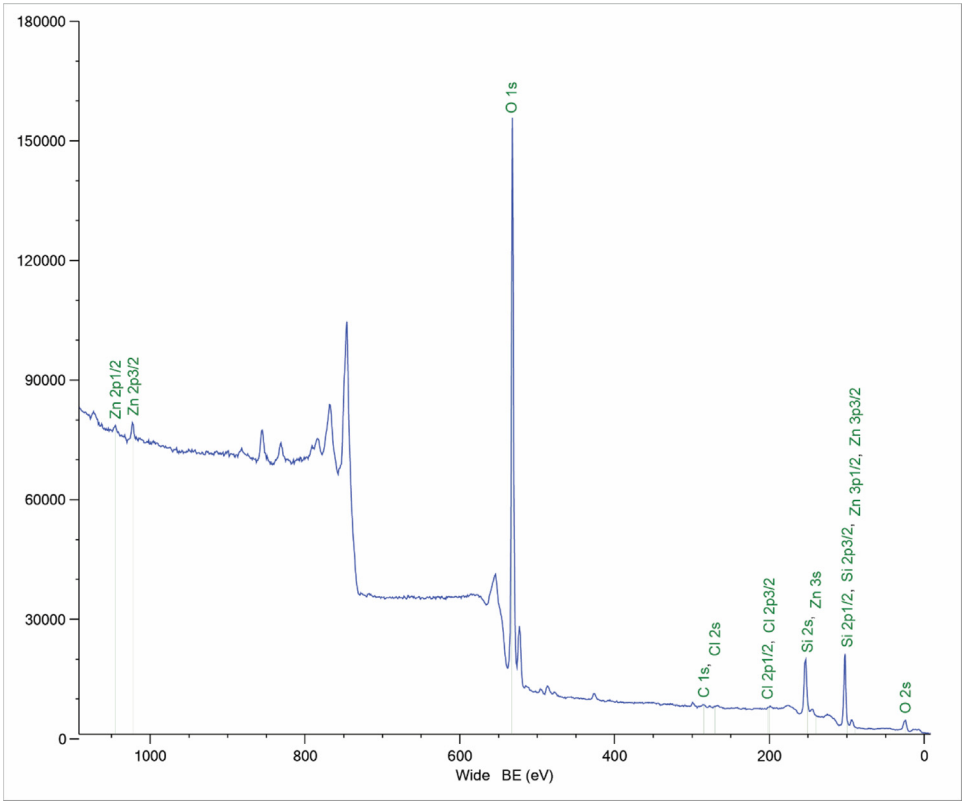

Fig. 11. XPS survey spectrum of **$ZnCl_2$-2.26@SiO_2** prepared by ball-milling of $ZnCl_2$ on **tt-$SiO_{2\text{-}150}$**.

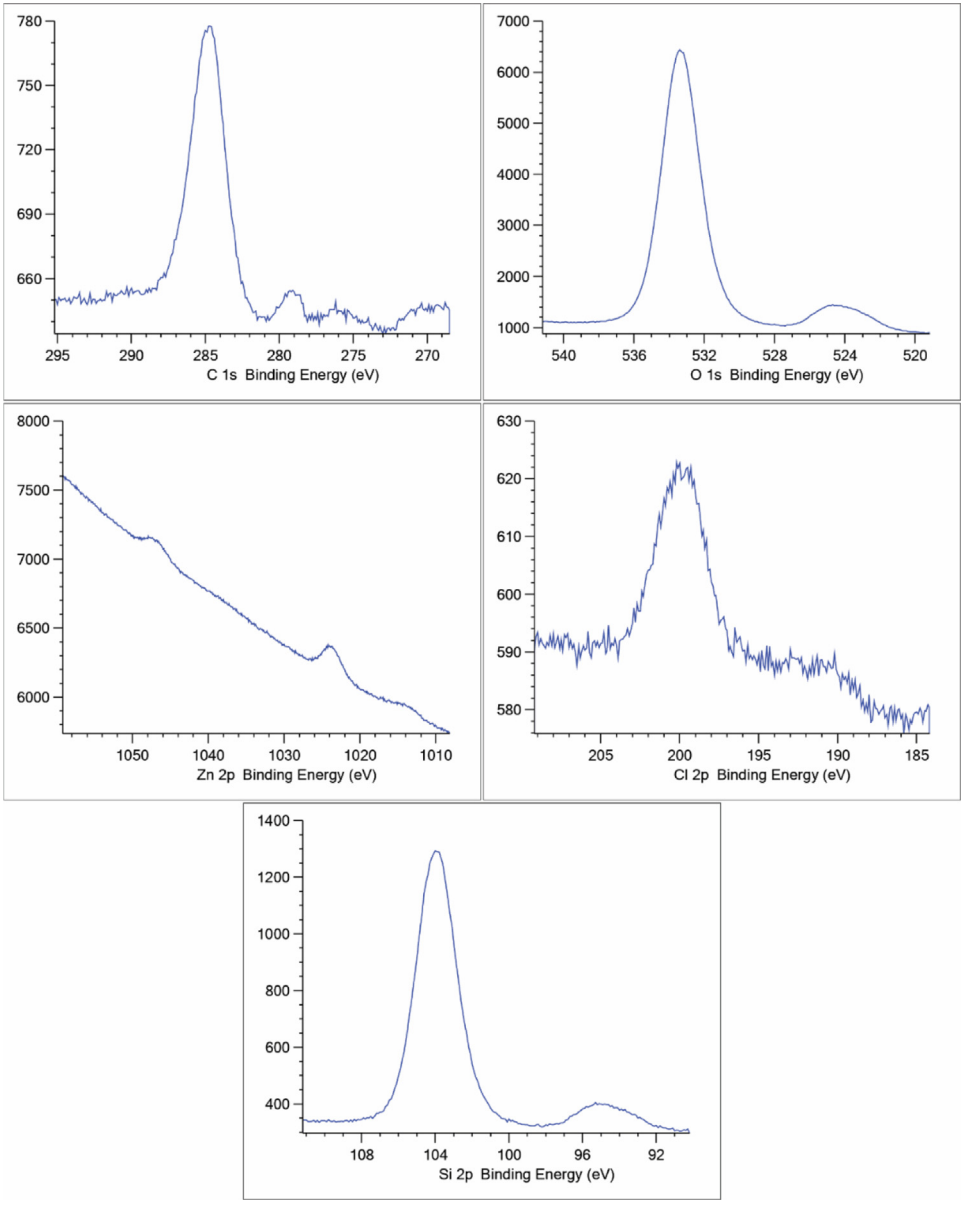

Fig. 12. High resolution XPS spectra of $ZnCl_2$-2.26@SiO_2 in the C 1s, O 1s, Zn 2p, Cl 2p and Si 2p spectral regions.

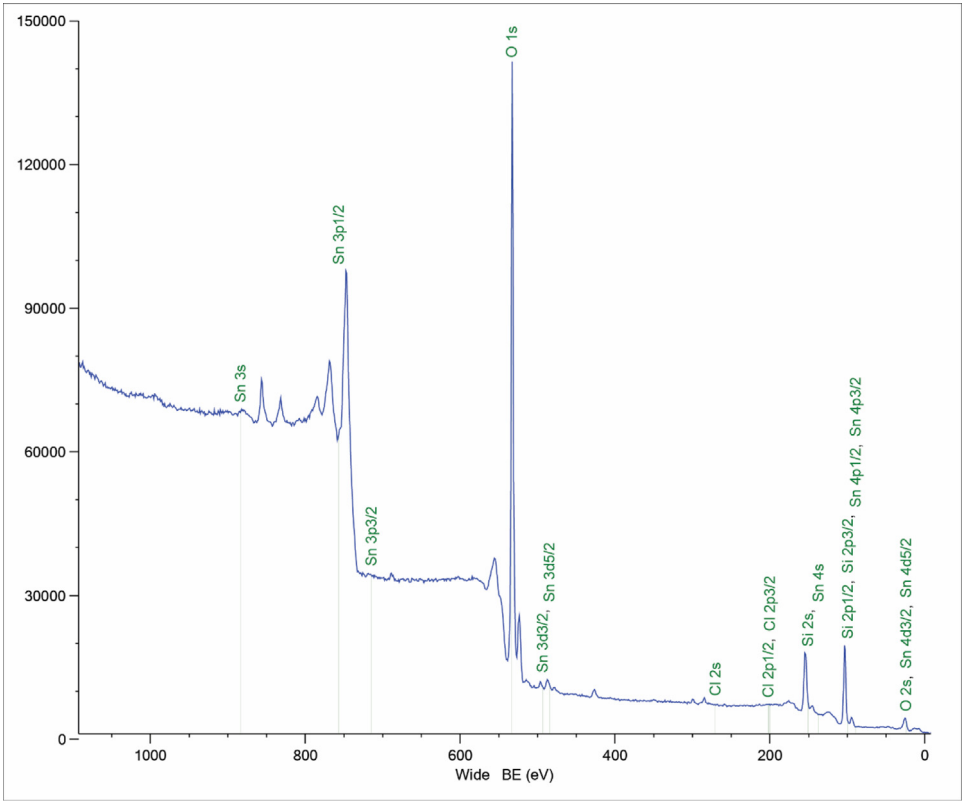

Fig. 13. XPS survey spectrum of **$SnCl_4$-0.84@SiO_2** prepared by impregnation of $SnCl_4$ on **tt-$SiO_{2\text{-}150}$**.

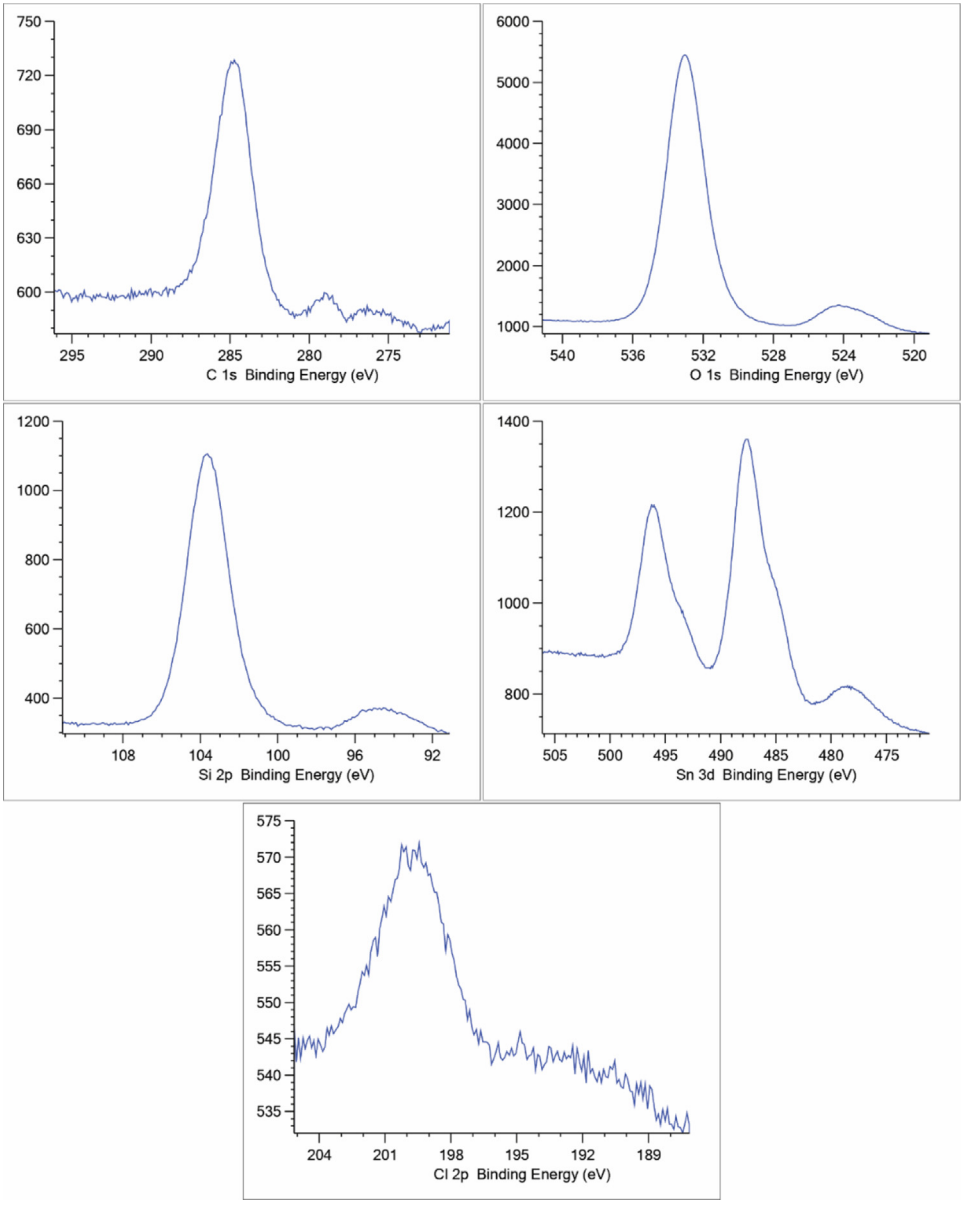

Fig. 14. High resolution XPS spectra of $SnCl_4$-0.84@SiO_2 in the C 1S, O 1s, Si 2p, Sn 3d and Cl 2p spectral regions.

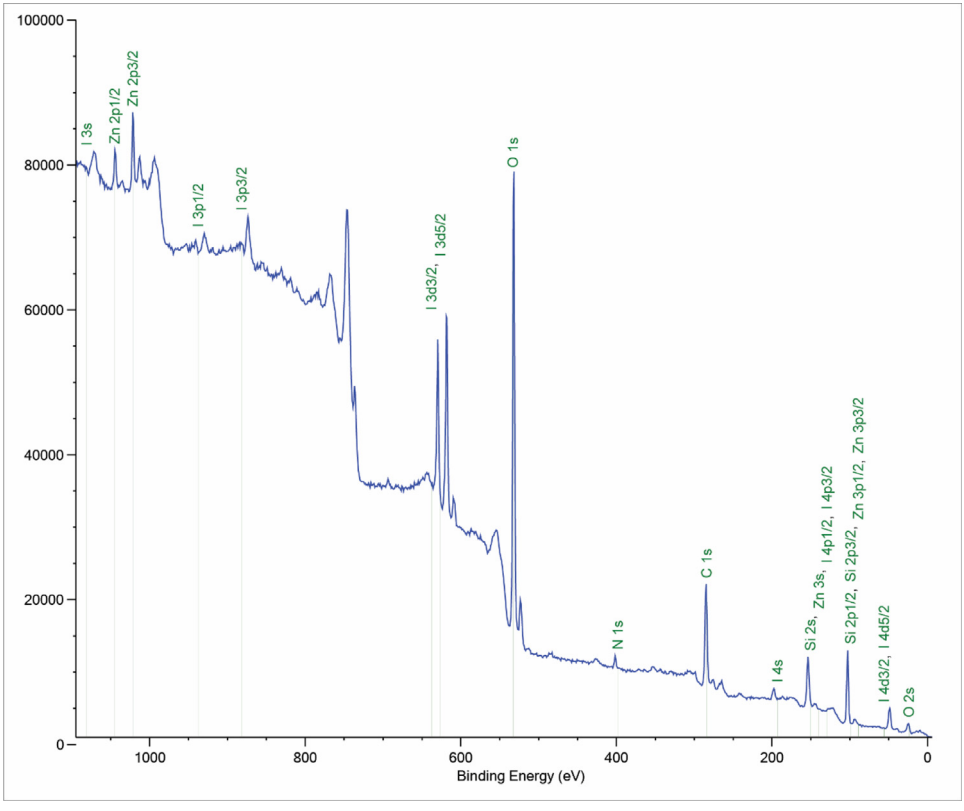

Fig. 15. XPS survey spectrum of **$ZnCl_2$(1.99)-IL-I** produced by grafting **IL-I** on **$ZnCl_2$-2.26@SiO_2**.

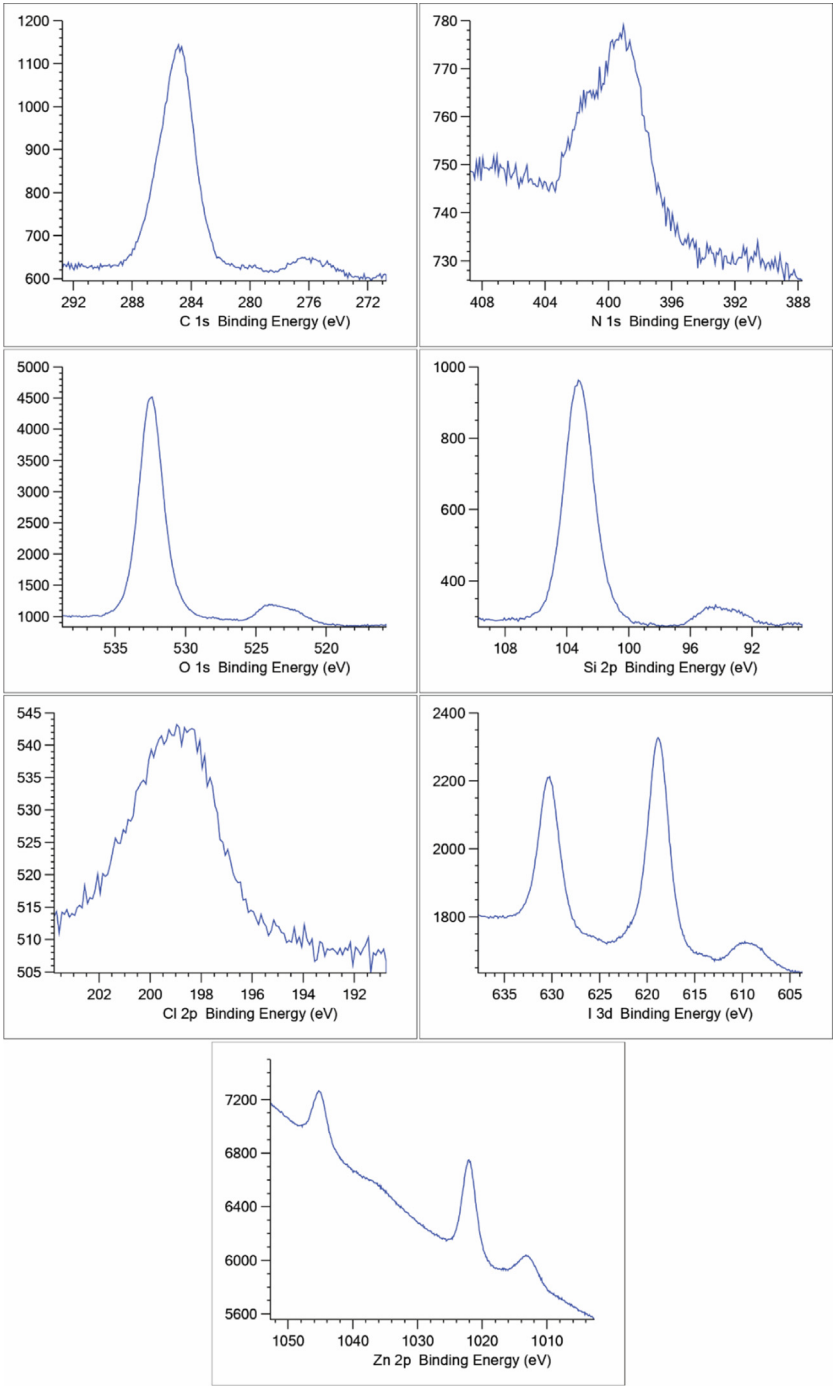

Fig. 16. High resolution XPS spectra of $ZnCl_2$(1.99)-IL-I in the C 1s, N 1s, O 1s, Si 2p, Cl 2p, I 3d and Zn 2p spectral regions.

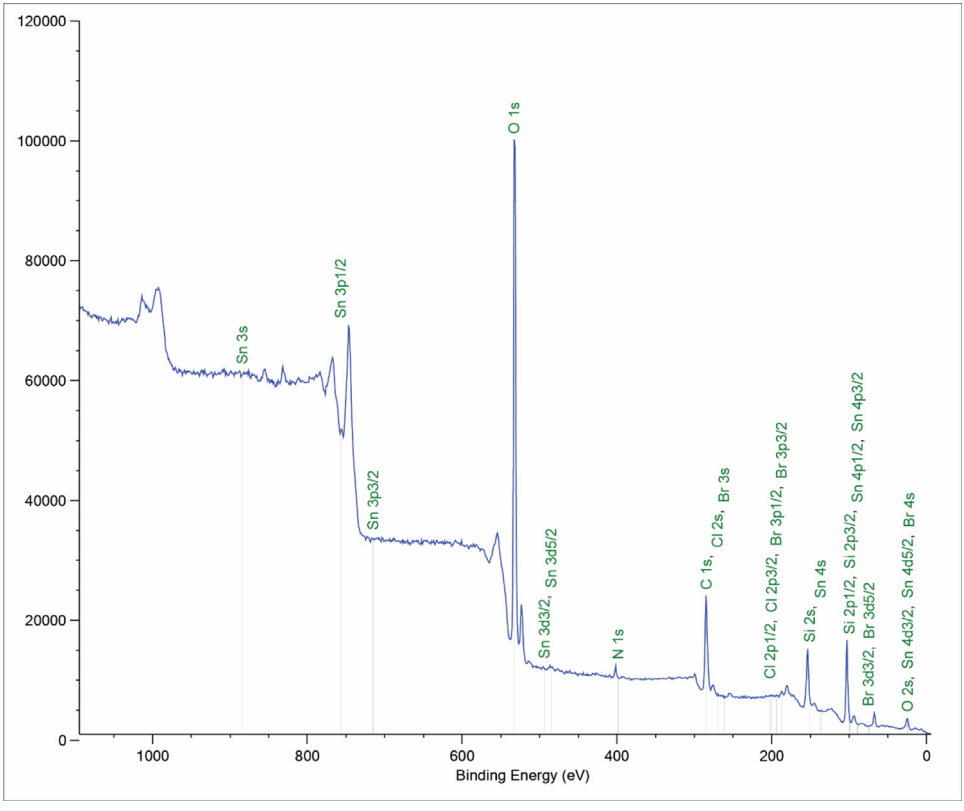

Fig. 17. XPS survey spectrum of **$SnCl_4$(0.66)-IL-Br** produced by the grafting of **IL-Br** on **$SnCl_4$-0.84@SiO_2**.

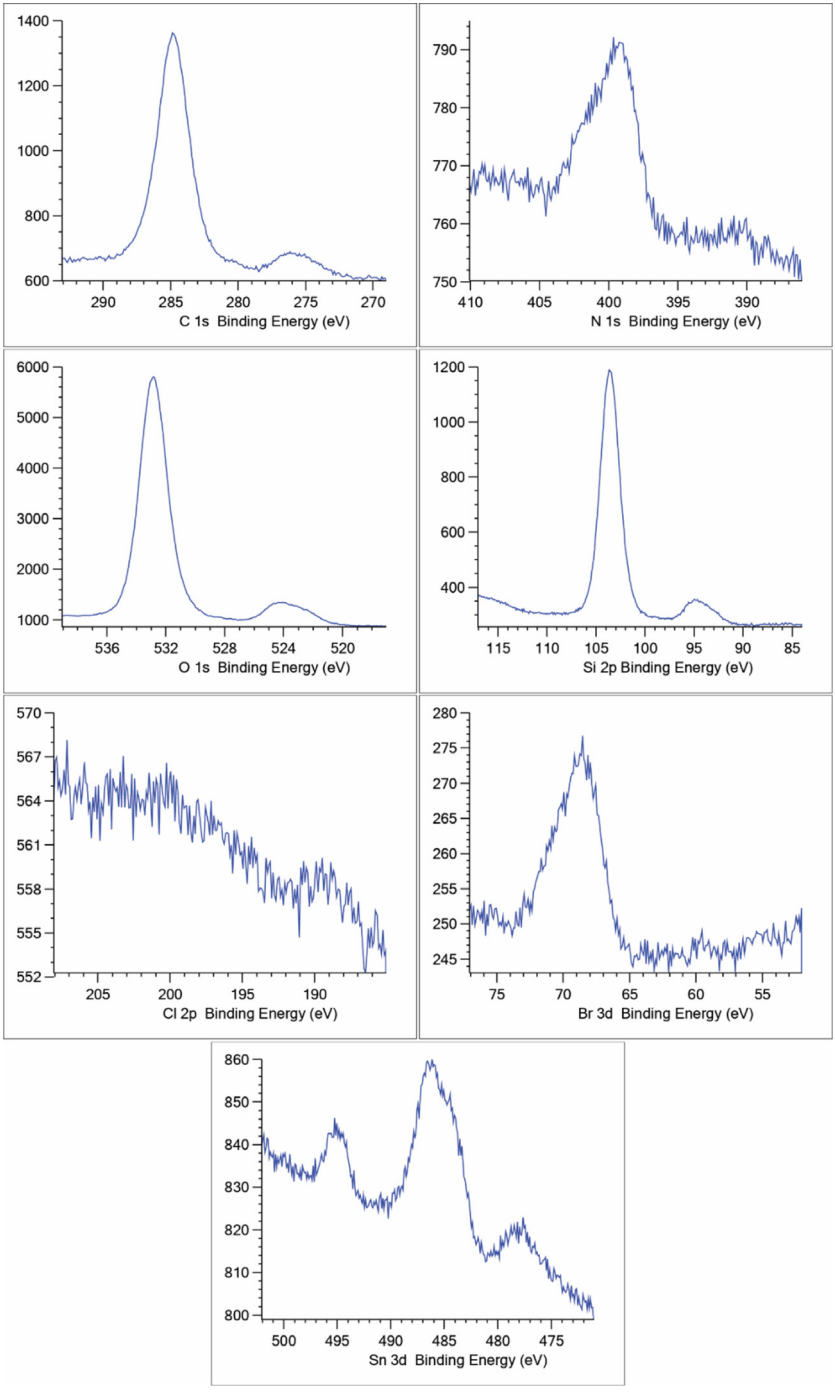

Fig. 18. High resolution XPS spectra of $SnCl_4$(0.66)-IL-Br in the C 1s, N 1s, O 1s, Si 2p, Cl 2p, Br 3d and Sn 3d spectral regions.

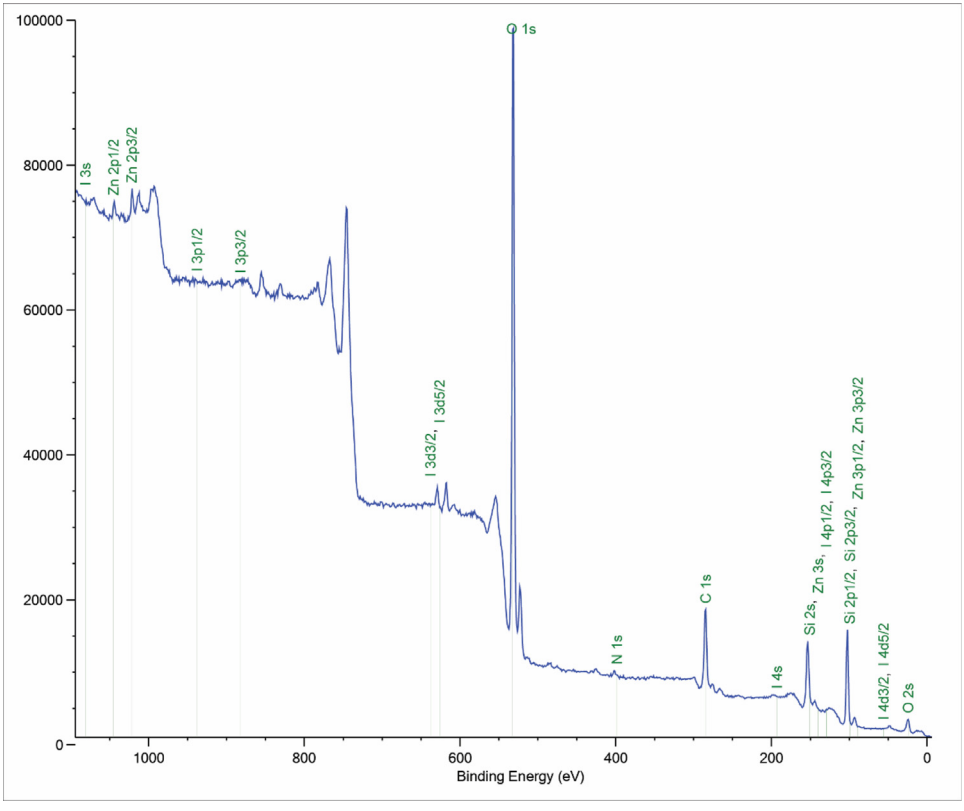

Fig. 19. XPS survey spectrum of spent $ZnCl_2$(1.99)-IL-I after five catalytic cycles.

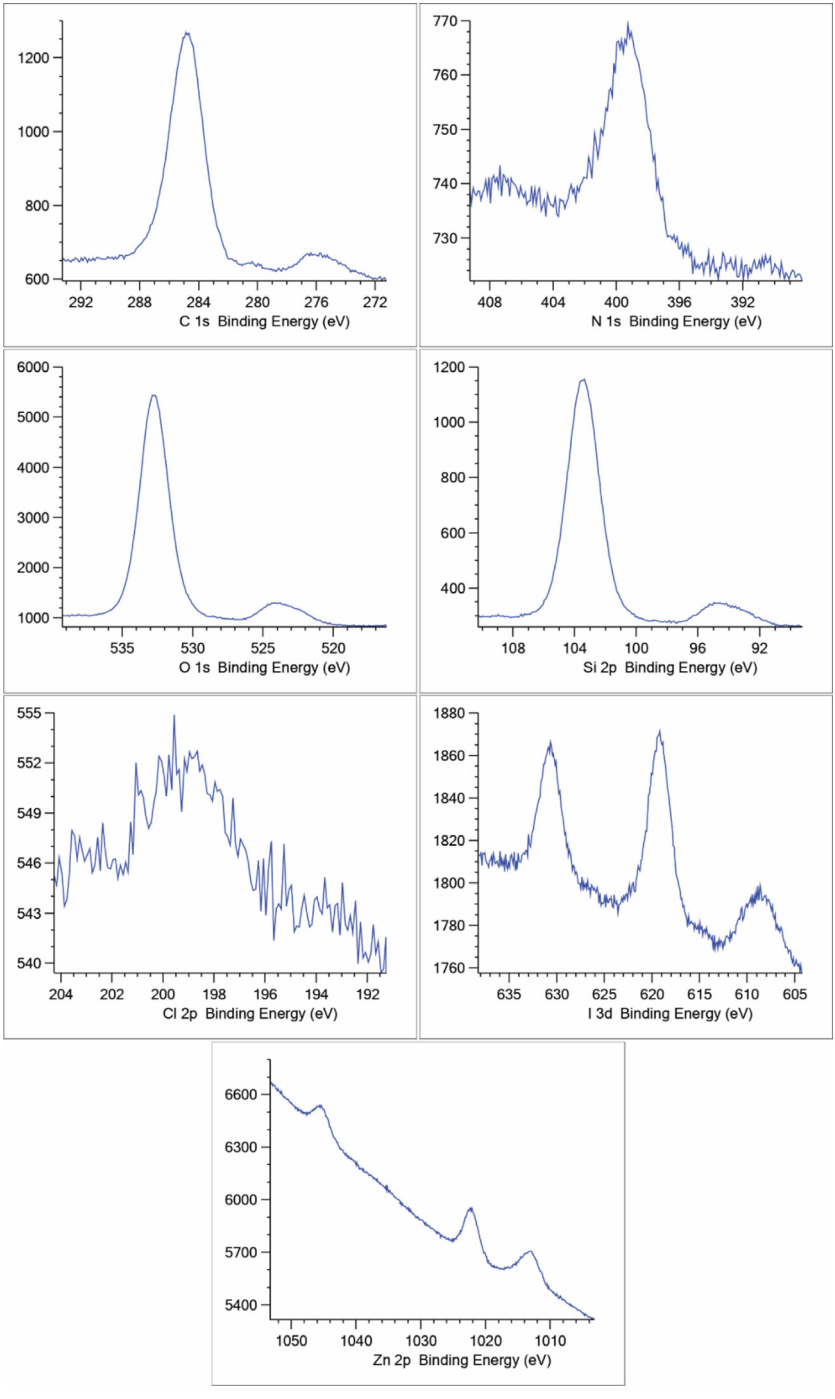

Fig. 20. High resolution XPS spectra of spent $ZnCl_2$(1.99)-IL-I in the C 1s, N 1s, O 1s, Si 2p, Cl 2p, I 3d and Zn 2p spectral regions.

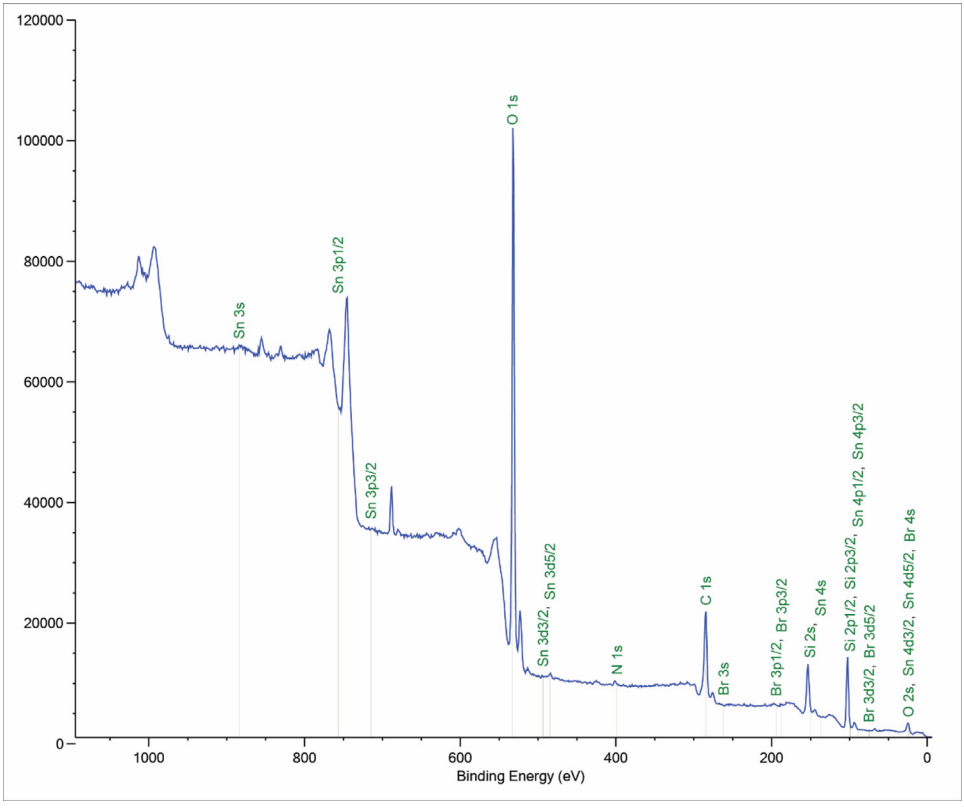

Fig. 21. XPS survey spectrum of spent $SnCl_4$(0.66)-IL-Br after five catalytic cycles.

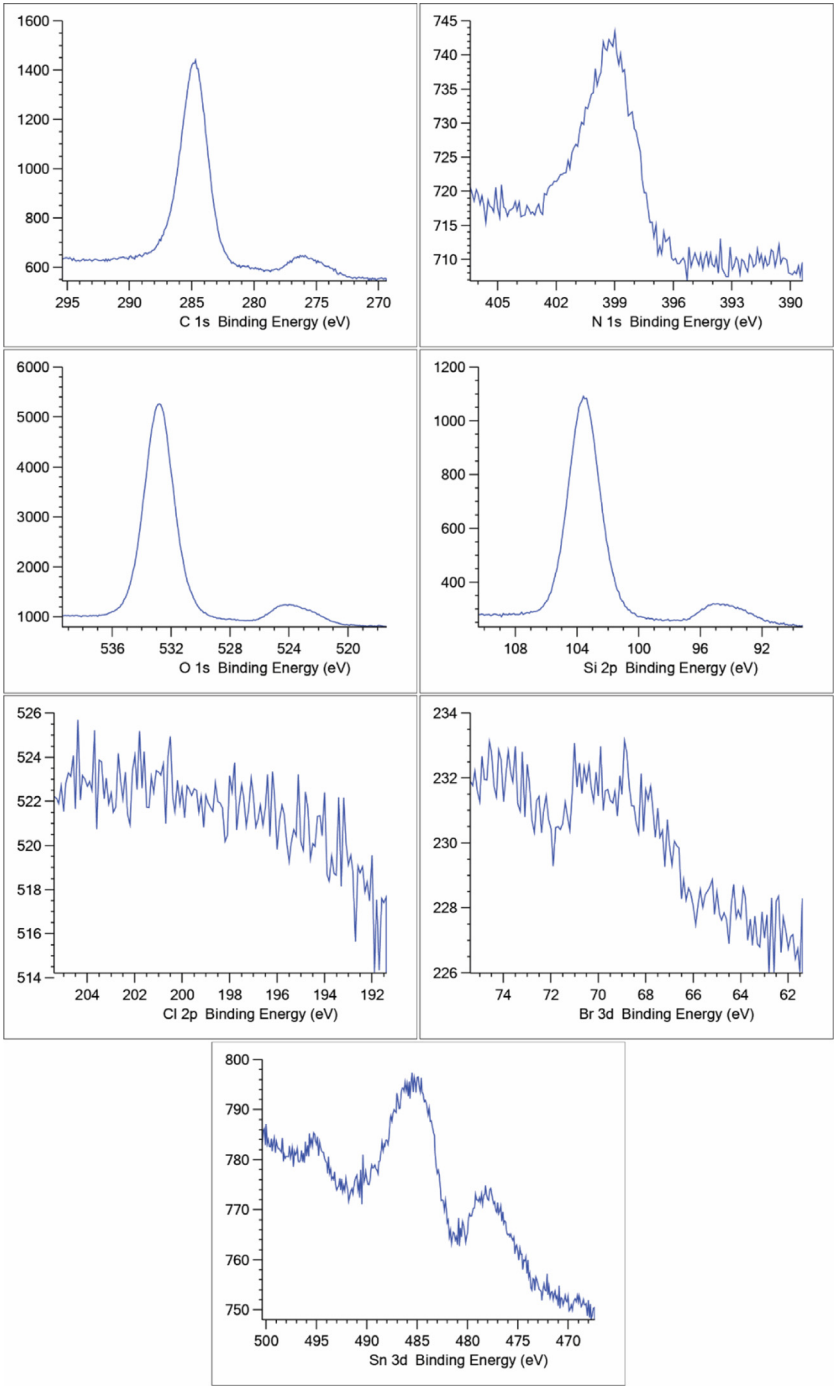

Fig. 22. High resolution XPS spectra of spent $SnCl_4$(0.66)-IL-Br in the C 1s, N 1s, O 1s, Si 2p, Cl 2p, Br 3d and Sn 3d spectral regions.

BET isotherms

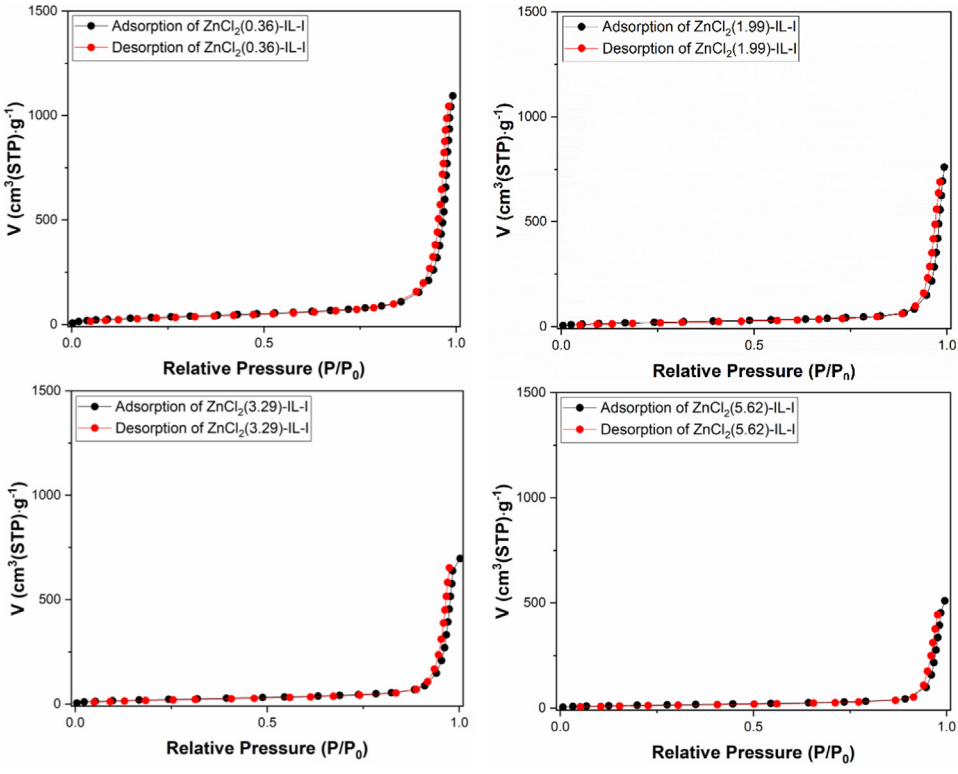

Fig. 23. BET adsorption/desorption isotherms of $ZnCl_2$-based materials (**$ZnCl_2$(0.36)-IL-I, $ZnCl_2$(1.99)-IL-I, $ZnCl_2$(3.29)-IL-I, $ZnCl_2$(5.62)-IL-I**) as indicated in the graphics.

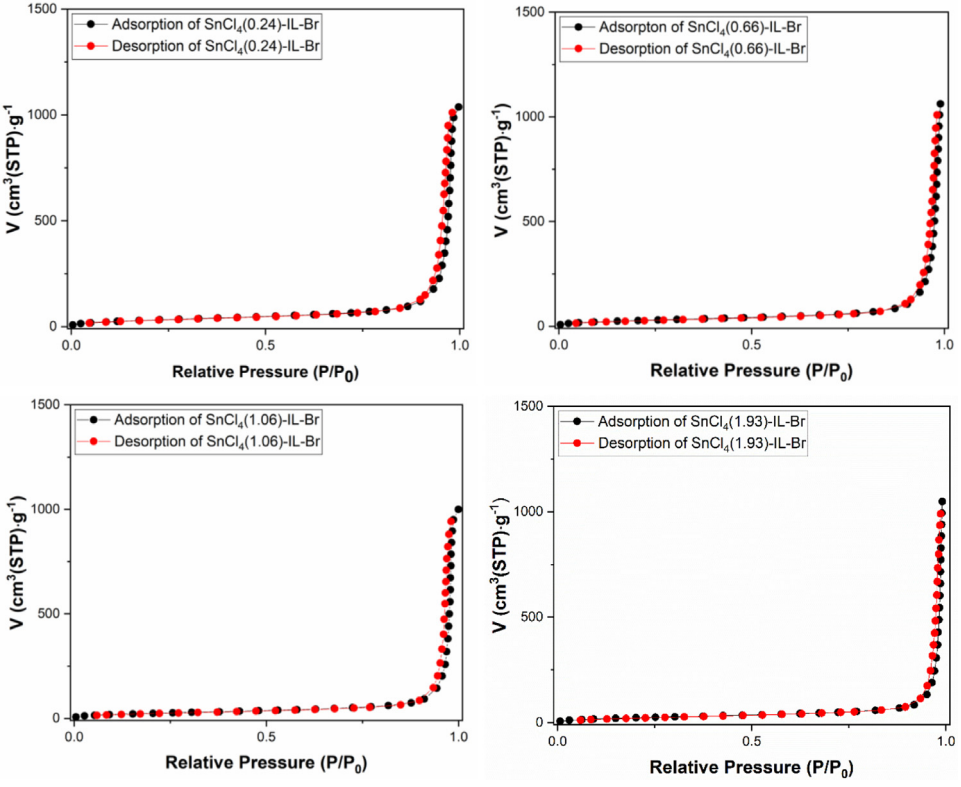

Fig. 24. BET adsorption/desorption isotherms of $SnCl_4$-based materials (**$SnCl_4$(0.24)-IL-Br, $SnCl_4$(0.66)-IL-Br, $SnCl_4$(1.06)-IL-Br, $SnCl_4$(1.93)-IL-Br**) as indicated in the graphics.

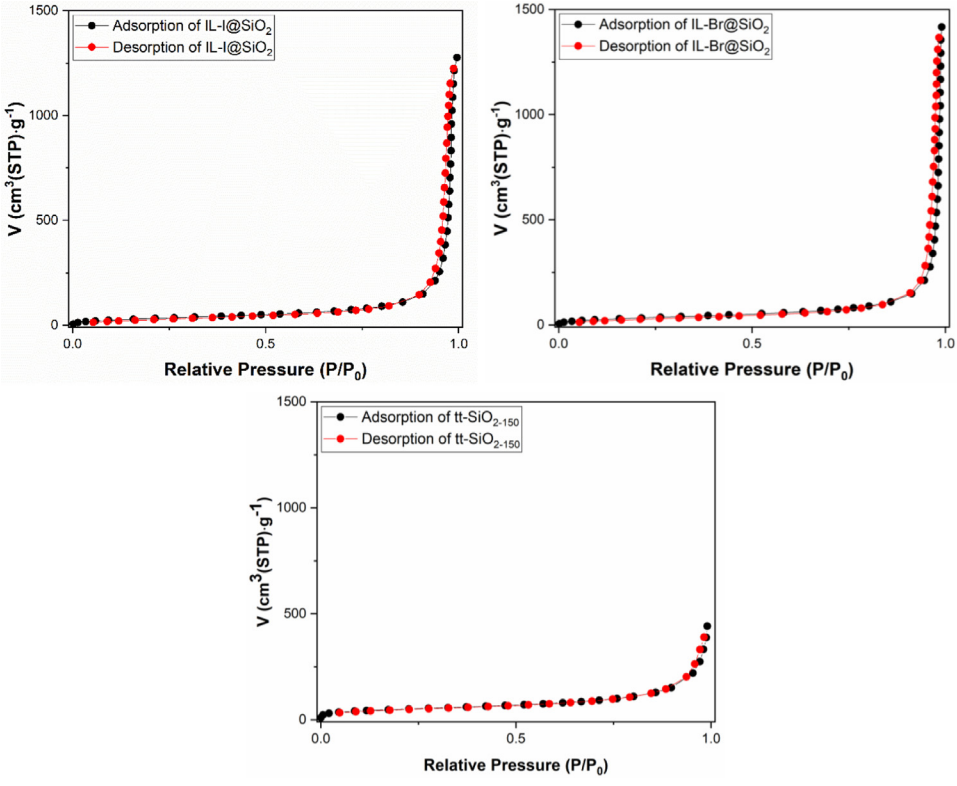

Fig. 25. BET adsorption/desorption isotherms of materials prepared without metal halides (**IL-I@SiO$_2$, IL-Br@SiO$_2$**) and of the **tt-SiO$_{2\text{-}150}$** support.

^{1}H NMR spectra of catalytic reactions

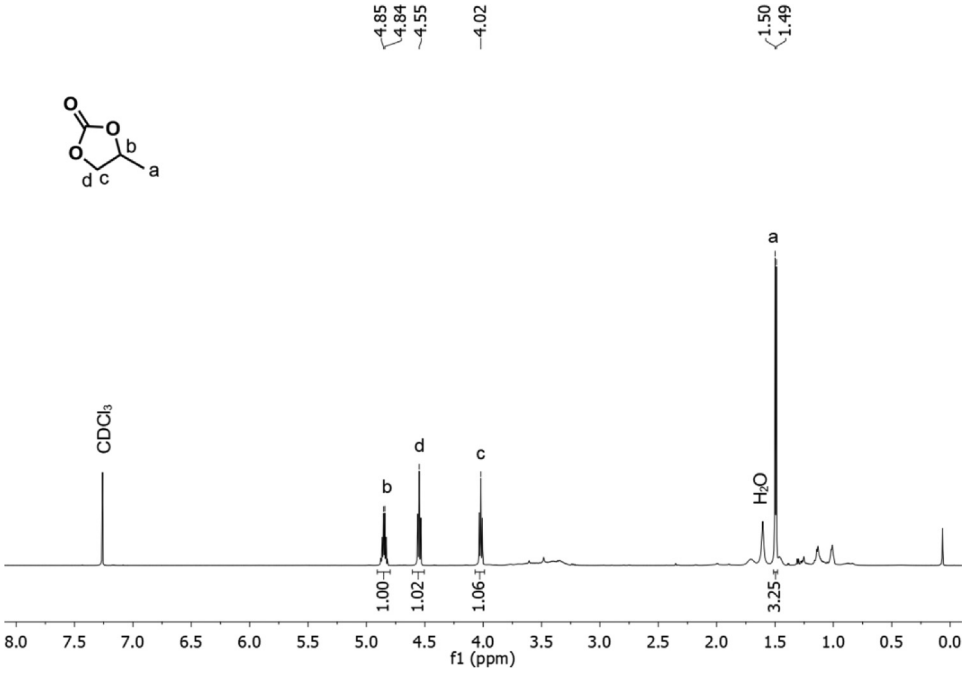

Fig. 26. ^{1}H-NMR spectrum of the cycloaddition of CO_2 to propylene oxide using 2 mol% **$ZnCl_2$(1.99)-IL-I** at room temperature, 1 bar CO_2 for 24 h.

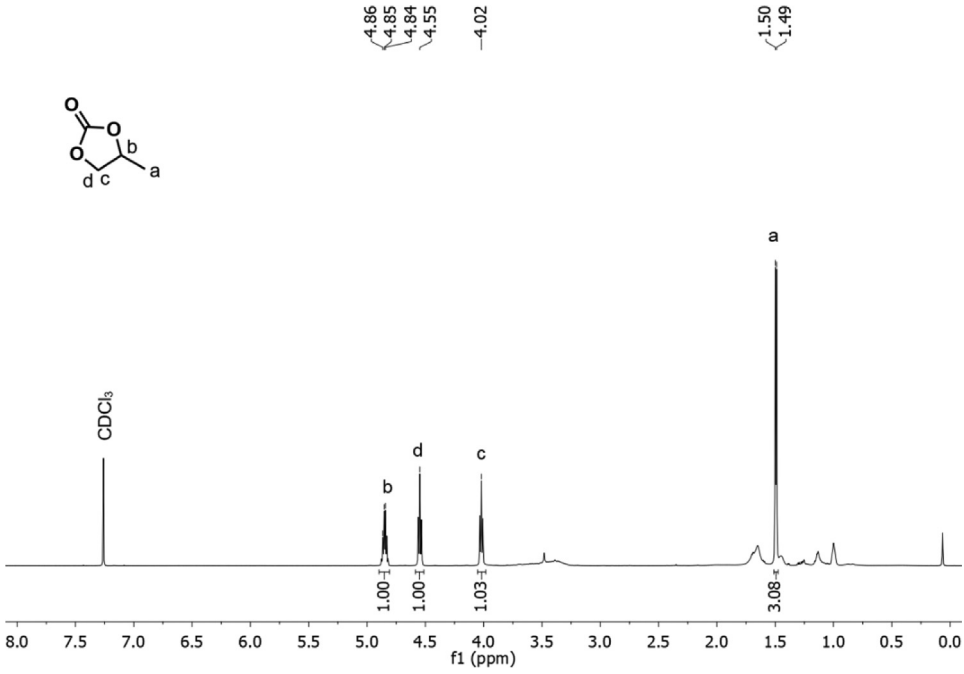

Fig. 27. ^{1}H-NMR spectrum of the cycloaddition of CO_2 to propylene oxide using 2 mol% **$SnCl_4$(0.66)-IL-Br** at room temperature, 1 bar CO_2 for 24 h.

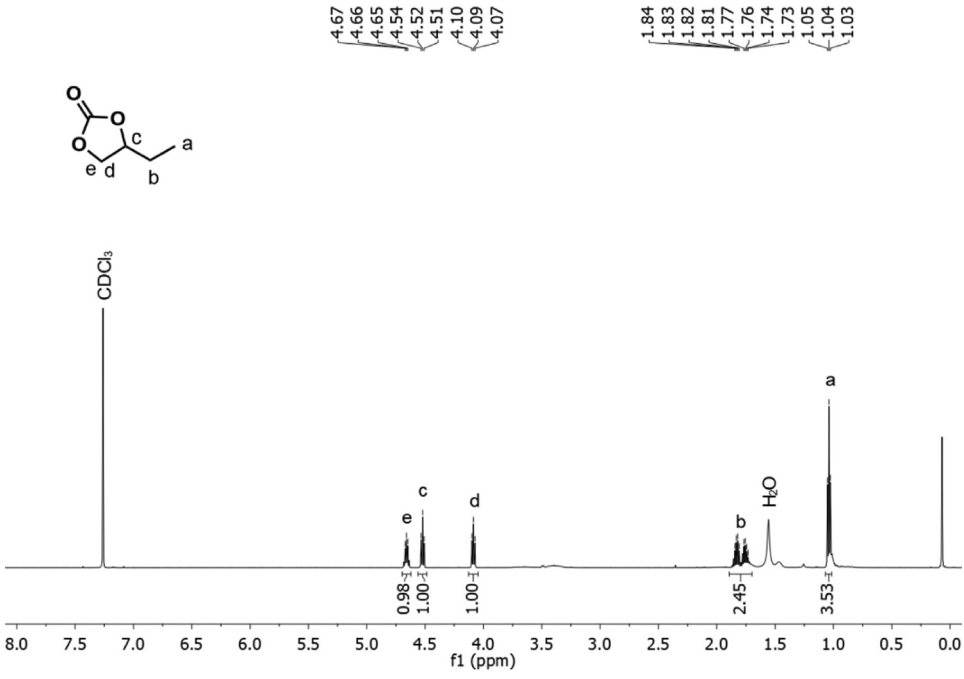

Fig. 28. ^{1}H-NMR spectrum of the cycloaddition of CO_2 to 1-butene oxide using 2 mol% **$ZnCl_2$(1.99)-IL-I** at room temperature, 1 bar CO_2 for 24 h.

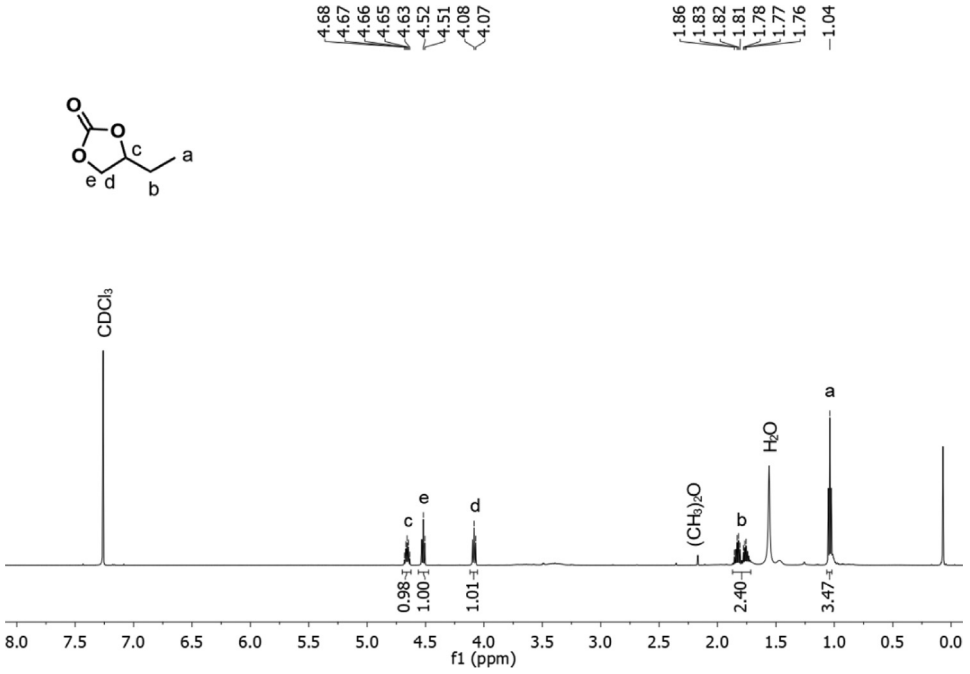

Fig. 29. [1]H-NMR spectrum of the cycloaddition of CO_2 to 1-butene oxide using 2 mol% **$SnCl_4$(0.66)-IL-Br** at room temperature, 1 bar CO_2 for 24 h.

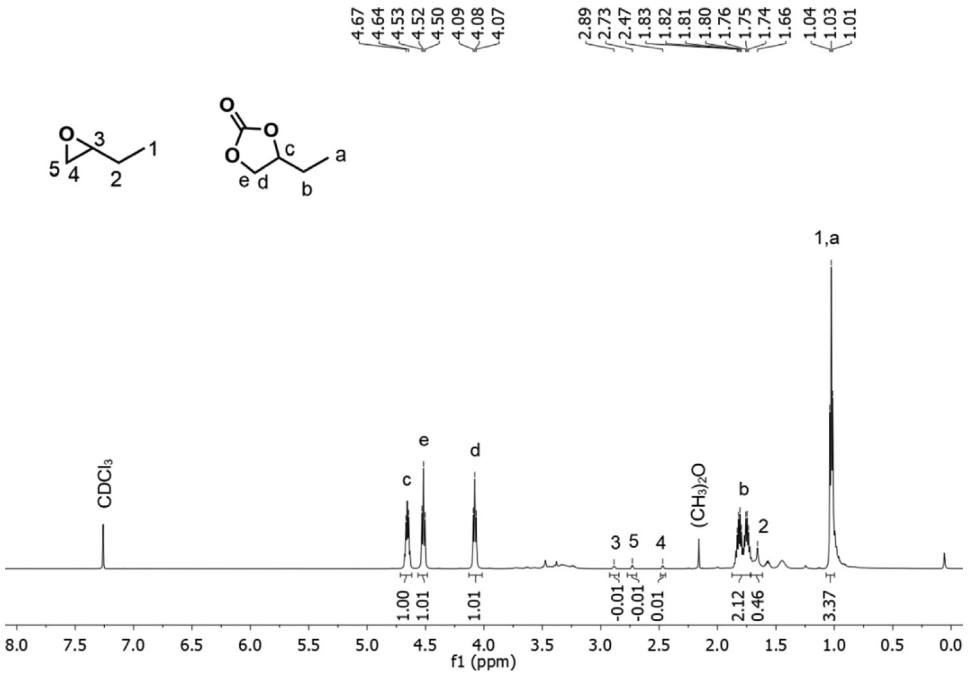

Fig. 30. [1]H-NMR spectrum of the cycloaddition of CO_2 to 1-butene oxide using 2 mol% **$ZnCl_2$(1.99)-IL-I** at room temperature, 1 bar CO_2 for 12 h.

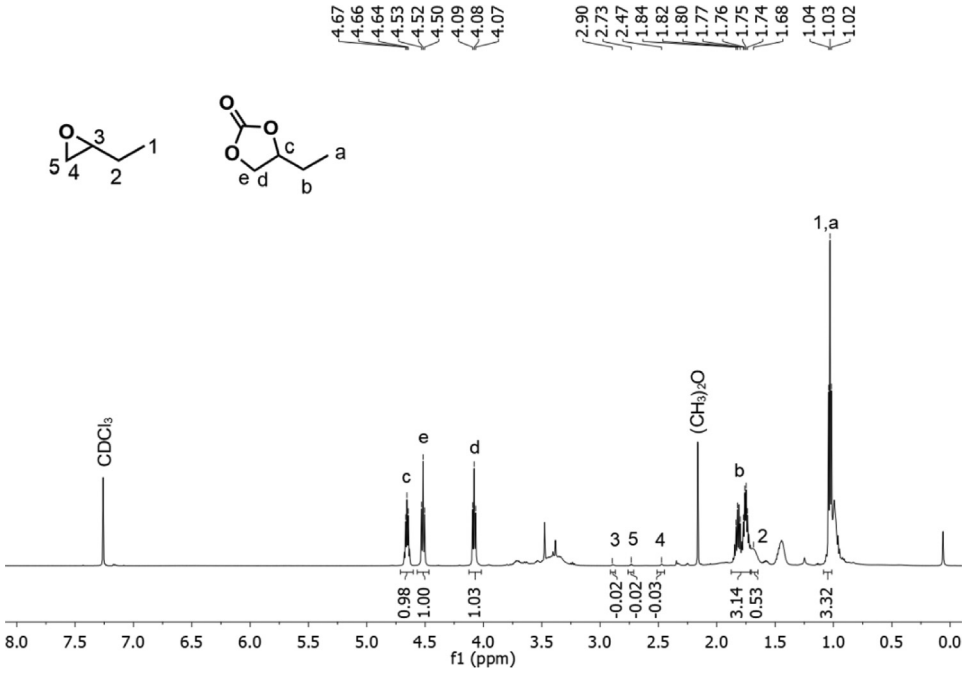

Fig. 31. [1]H-NMR spectrum of the cycloaddition of CO_2 to 1-butene oxide using 2 mol% **$SnCl_4$(0.66)-IL-Br** at room temperature, 1 bar CO_2 for 12 h.

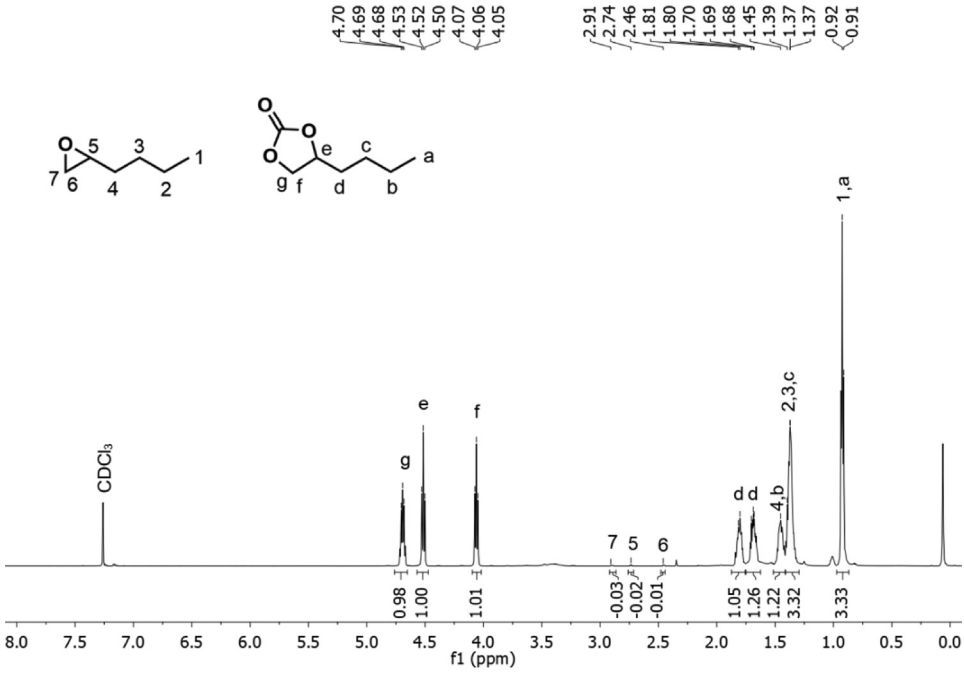

Fig. 32. [1]H-NMR spectrum of the cycloaddition of CO_2 to 1-hexene oxide using 2 mol% **$ZnCl_2$(1.99)-IL-I** at 40°C, 1 bar CO_2 for 24 h.

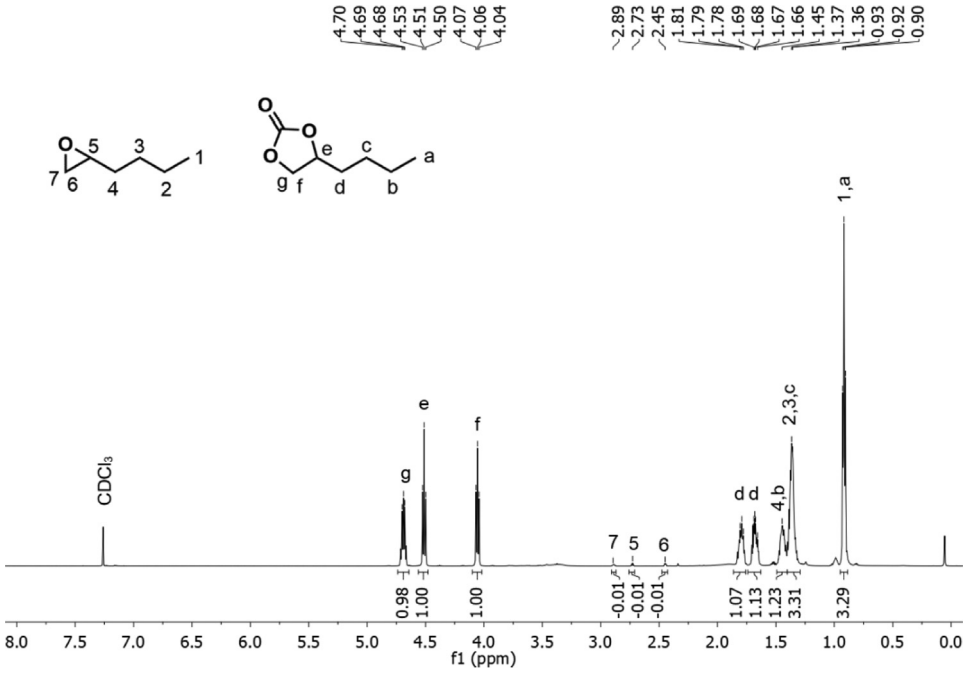

Fig. 33. [1]H-NMR spectrum of the cycloaddition of CO_2 to 1-hexene oxide using 2 mol% **$SnCl_4$(0.66)-IL-Br** at room temperature, 1 bar CO_2 for 4 h.

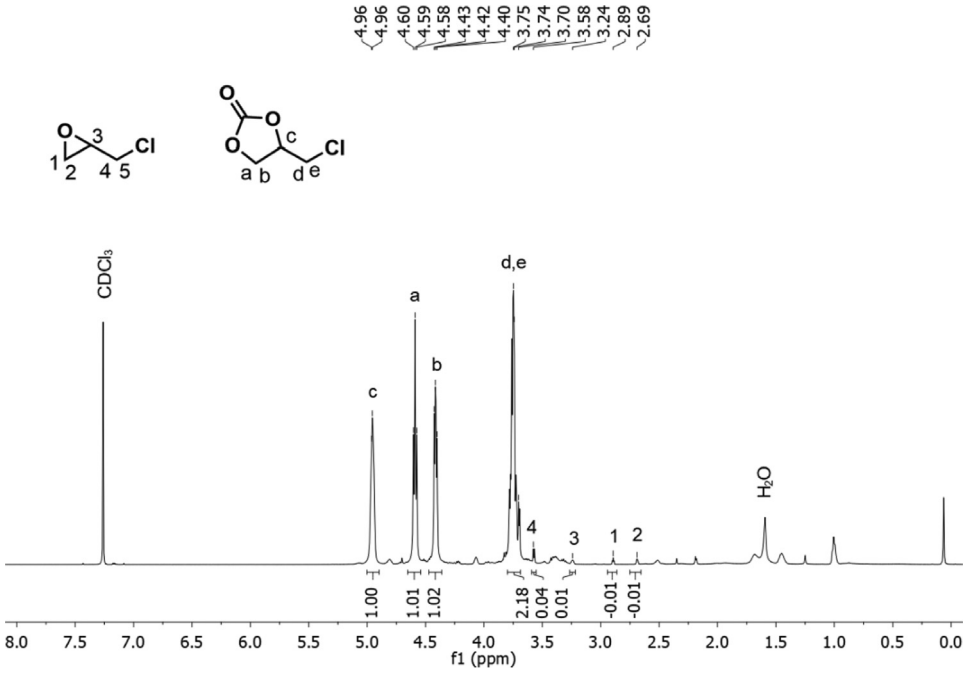

Fig. 34. [1]H-NMR spectrum of the cycloaddition of CO_2 to epichlorohydrin using 2 mol% **$ZnCl_2$(1.99)-IL-I** at 40°C, 1 bar CO_2 for 24 h.

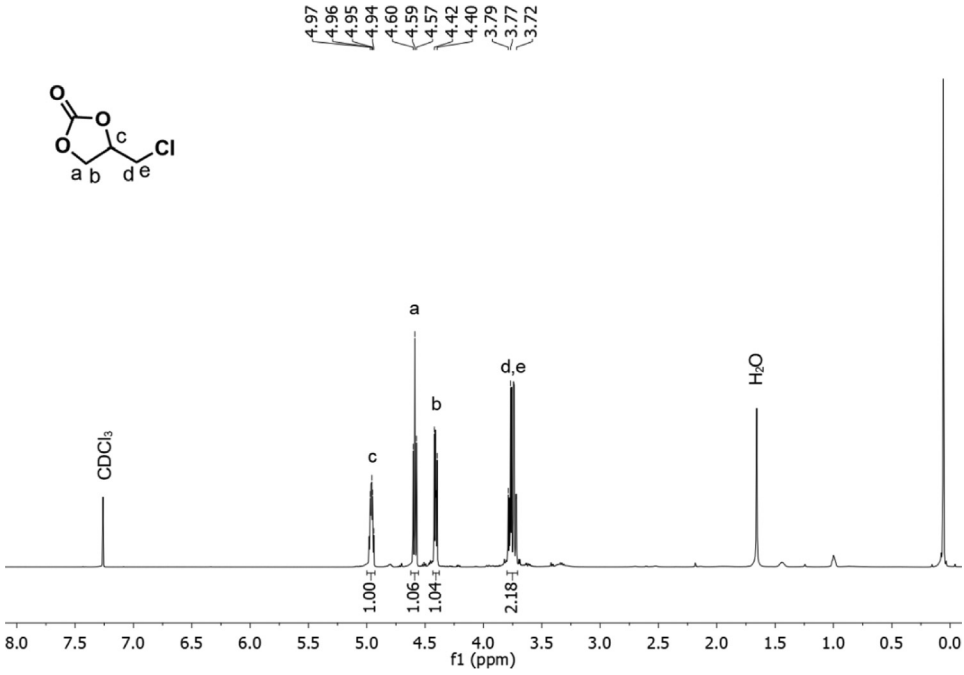

Fig. 35. ^{1}H-NMR spectrum of the cycloaddition of CO_2 to epichlorohydrin using 2 mol% **$SnCl_4$(0.66)-IL-Br** at room temperature, 1 bar CO_2 for 24 h.

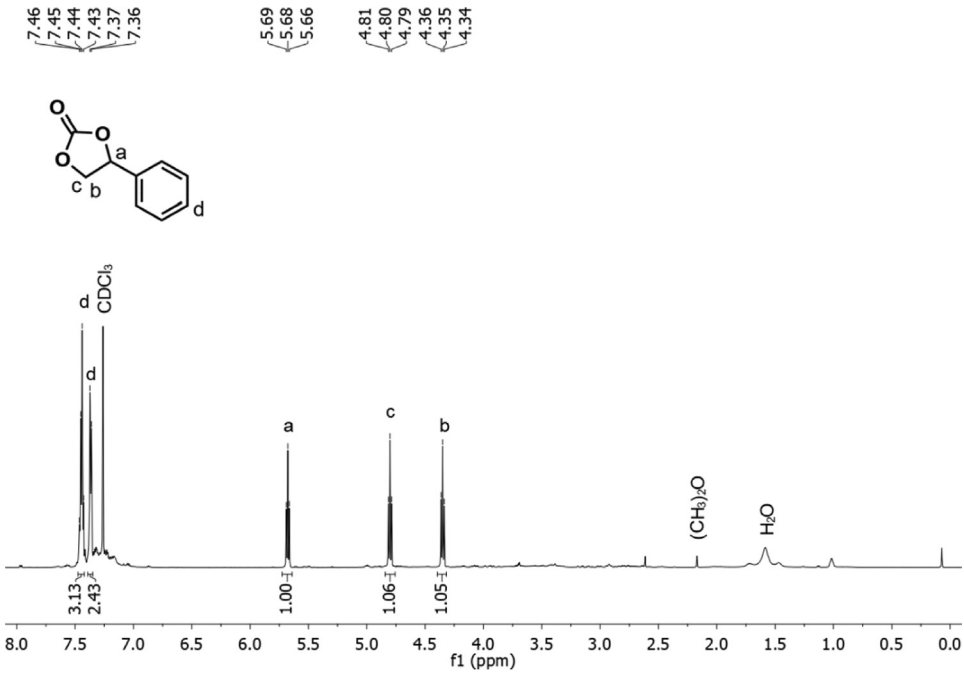

Fig. 36. ^{1}H-NMR spectrum of the cycloaddition of CO_2 to styrene oxide using 2 mol% **$ZnCl_2$(1.99)-IL-I** at 40°C, 1 bar CO_2 for 24 h.

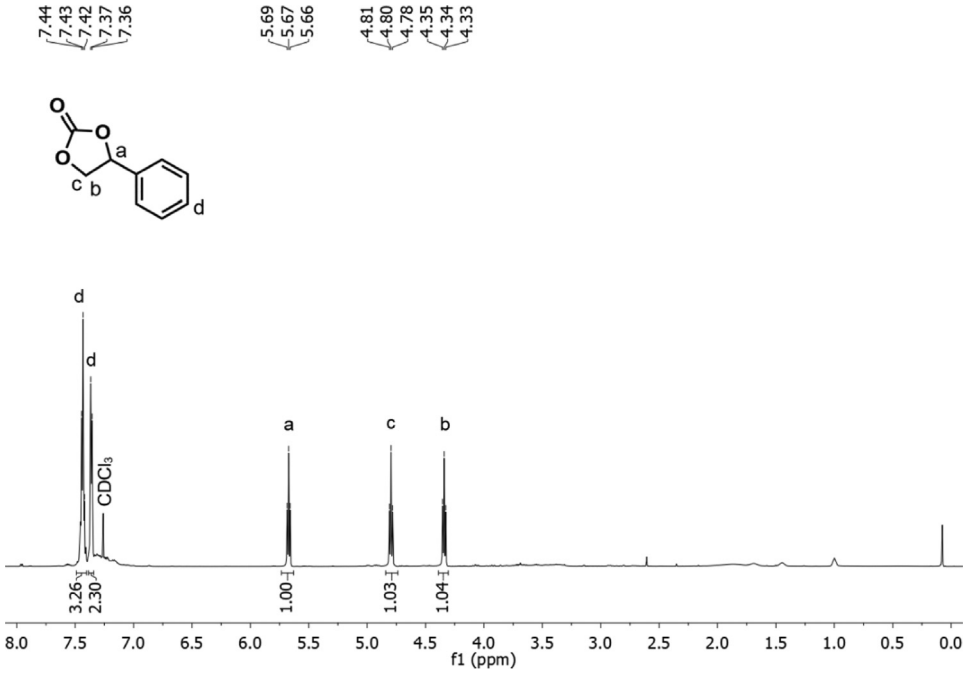

Fig. 37. ^{1}H-NMR spectrum of the cycloaddition of CO_2 to styrene oxide using 2 mol% **$SnCl_4$(0.66)-IL-Br** at 40°C, 1 bar CO_2 for 48 h.

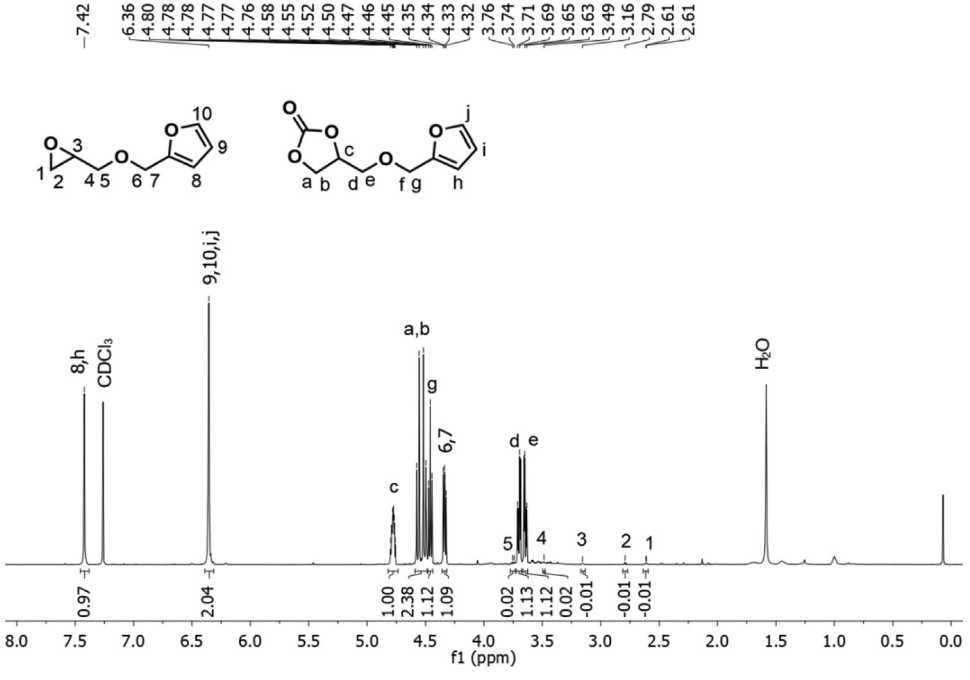

Fig. 38. ^{1}H-NMR spectrum of the cycloaddition of CO_2 to furfuryl glycidyl ether using 2 mol% **$ZnCl_2$(1.99)-IL-I** at 40°C, 1 bar CO_2 for 24 h.

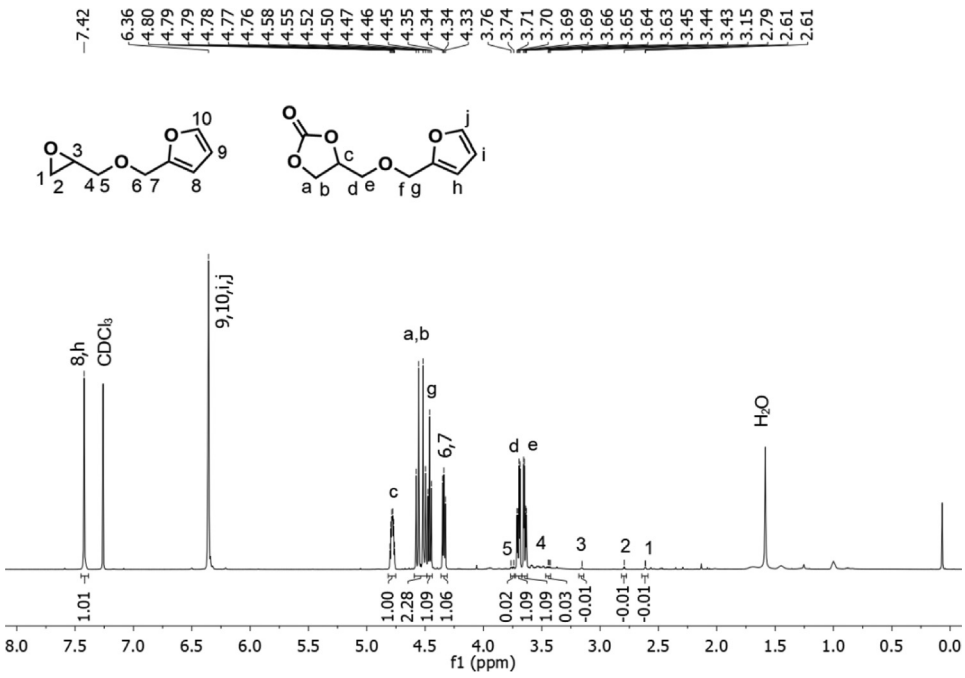

Fig. 39. ^{1}H-NMR spectrum of the cycloaddition of CO_2 to furfuryl glycidyl ether using 2 mol% **$SnCl_4$(0.66)-IL-Br** at 40°C, 1 bar CO_2 for 24 h.

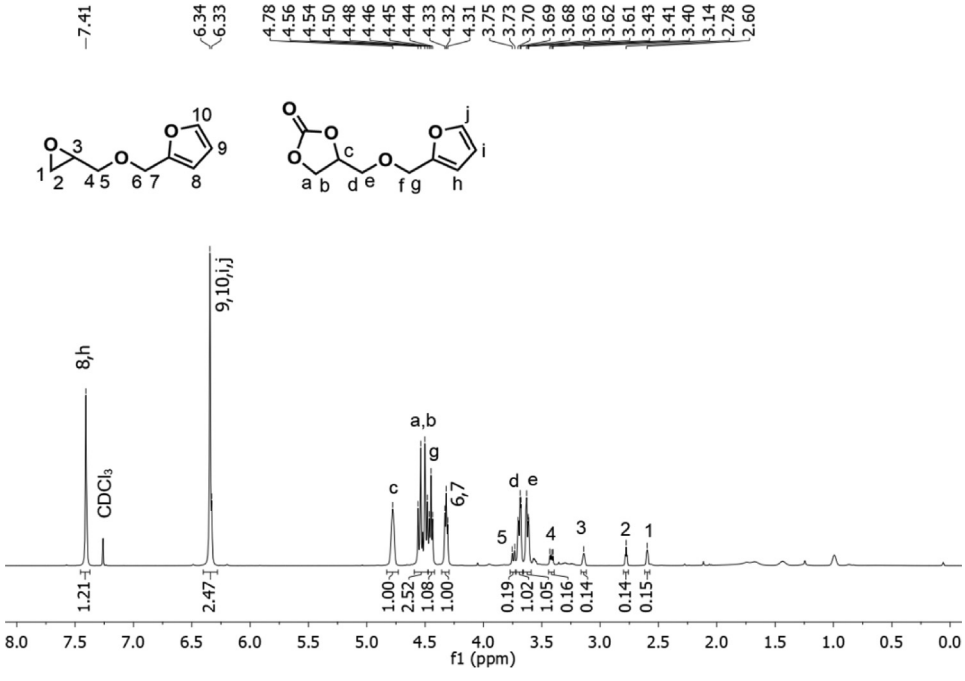

Fig. 40. ^{1}H-NMR spectrum of the cycloaddition of CO_2 to furfuryl glycidyl ether using 2 mol% **$ZnCl_2$(1.99)-IL-I** at 40°C, 1 bar CO_2 for 12 h.

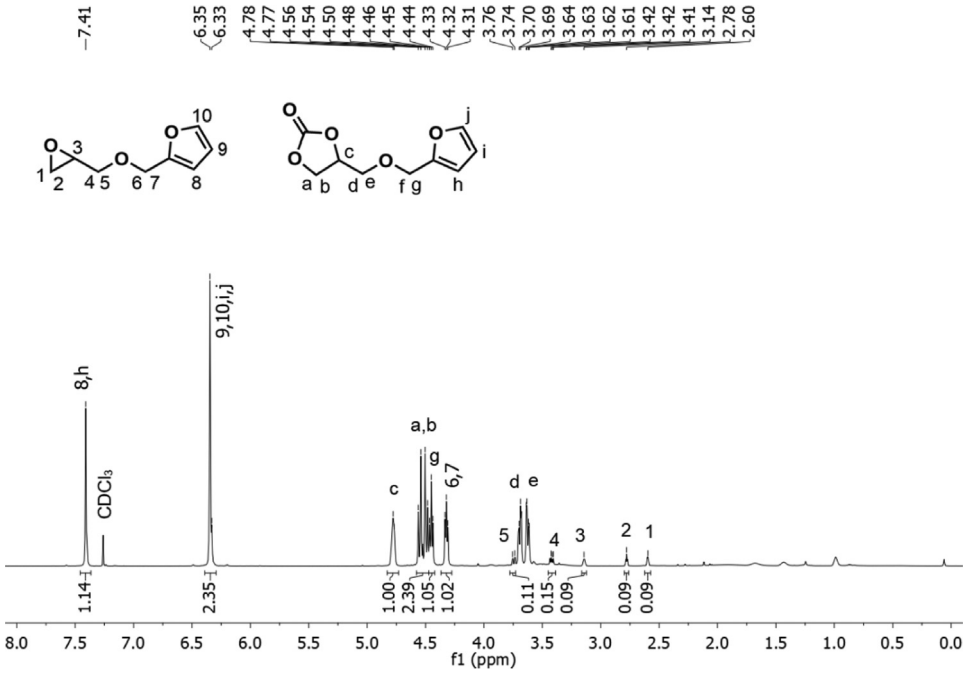

Fig. 41. ^{1}H-NMR spectrum of the cycloaddition of CO_2 to furfuryl glycidyl ether using 2 mol% **$SnCl_4$(0.66)-IL-Br** at 40°C, 1 bar CO_2 for 12 h.

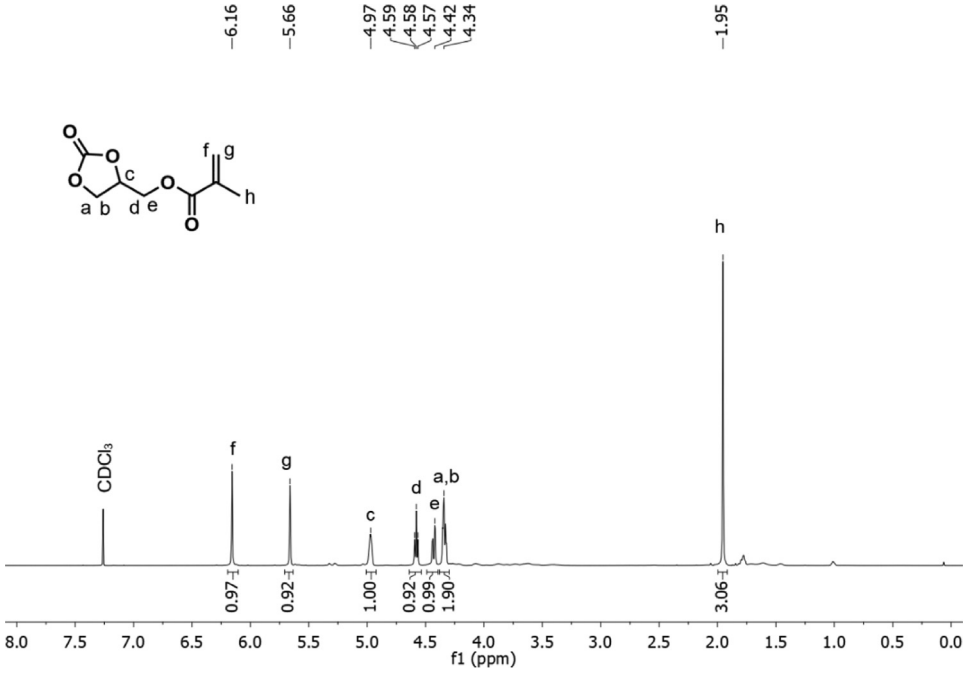

Fig. 42. ^{1}H-NMR spectrum of the cycloaddition of CO_2 to glycidyl methacrylate using 2 mol% **$ZnCl_2$(1.99)-IL-I** at 40°C, 1 bar CO_2 for 24 h.

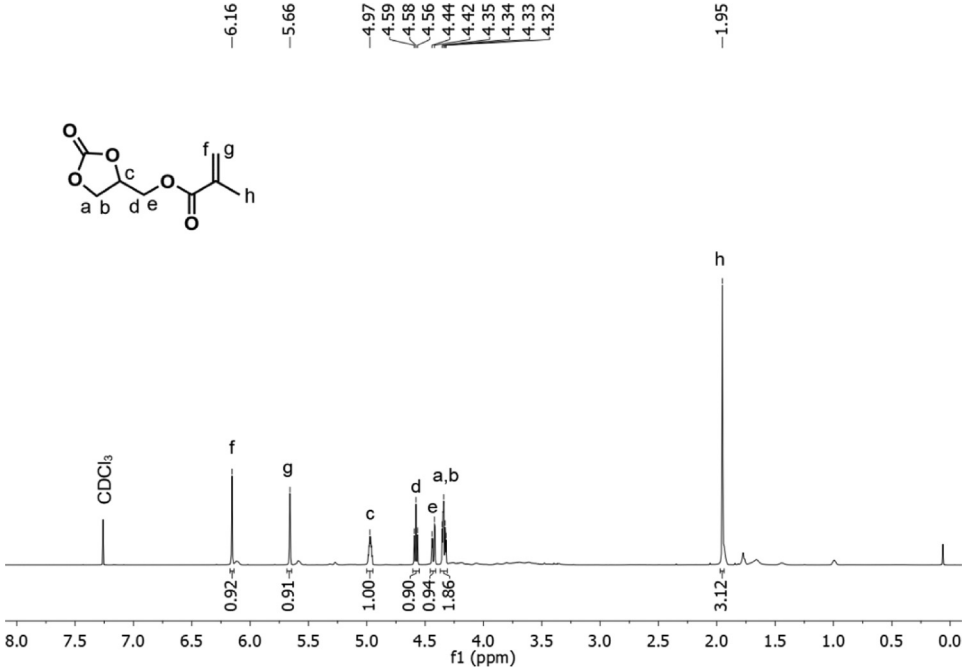

Fig. 43. ^{1}H-NMR spectrum of the cycloaddition of CO_2 to glycidyl methacrylate using 2 mol% **$SnCl_4$(0.66)-IL-Br** at 40°C, 1 bar CO_2 for 24 h.

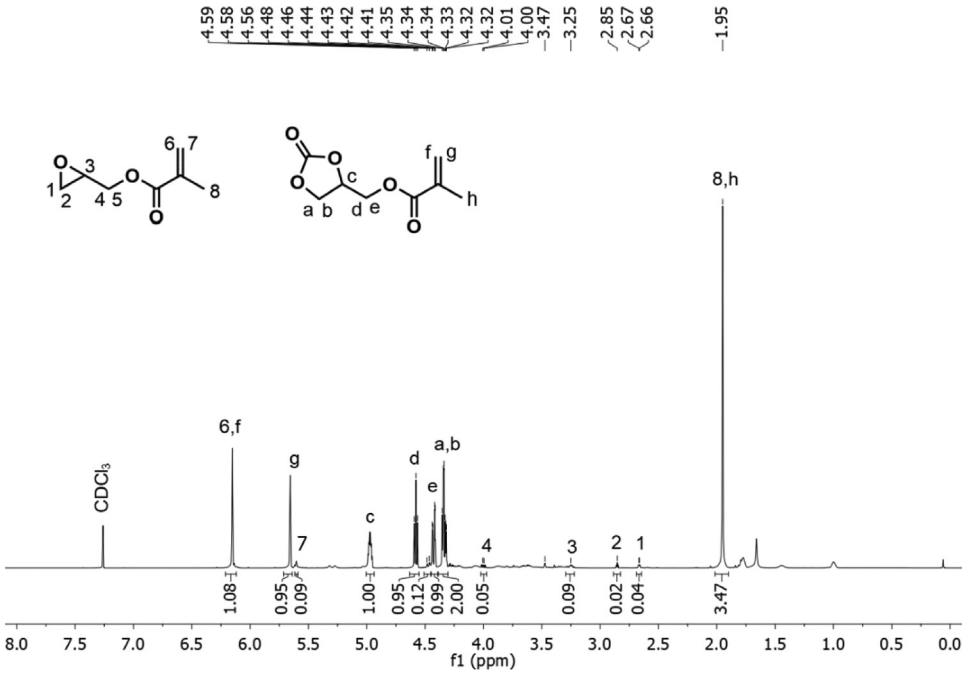

Fig. 44. ^{1}H-NMR spectrum of the cycloaddition of CO_2 to glycidyl methacrylate using 2 mol% **$ZnCl_2$(1.99)-IL-I** at 40°C, 1 bar CO_2 for 12 h.

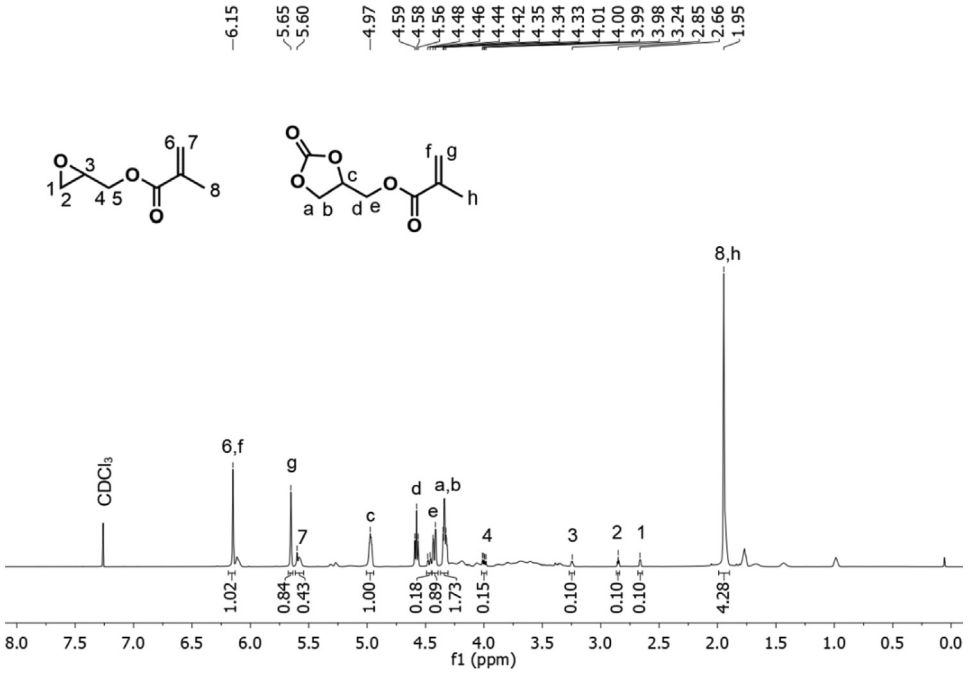

Fig. 45. ^{1}H-NMR spectrum of the cycloaddition of CO_2 to glycidyl methacrylate using 2 mol% **$SnCl_4$(0.66)-IL-Br** at 40°C, 1 bar CO_2 for 12 h.

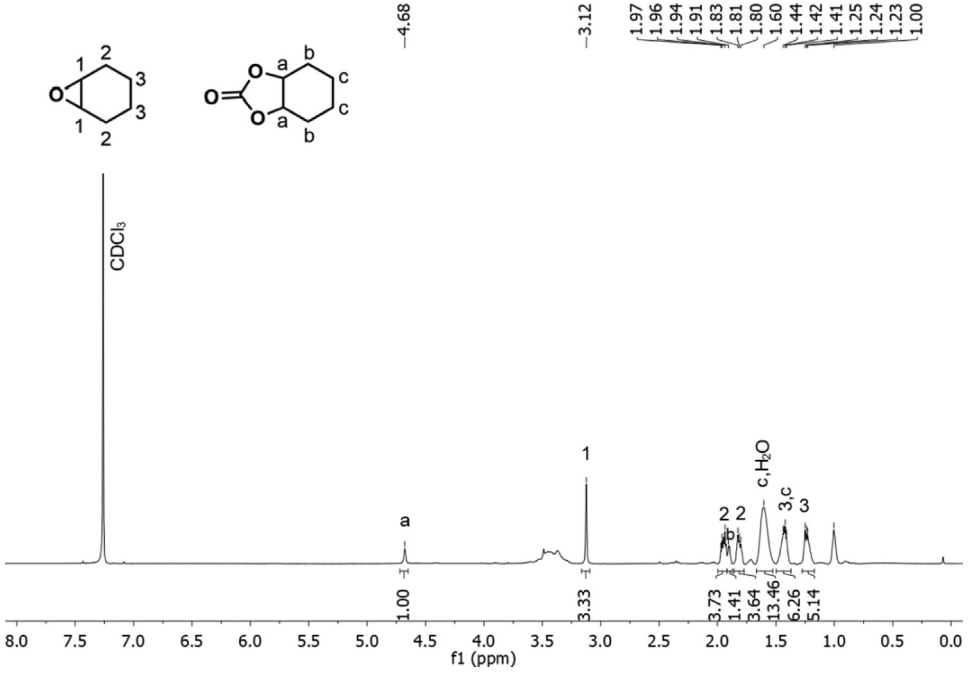

Fig. 46. ^{1}H-NMR spectrum of the cycloaddition of CO_2 to epoxy cyclohexane using 2 mol% **$ZnCl_2$(1.99)-IL-I** at 100°C, 15 bar CO_2 for 48 h.

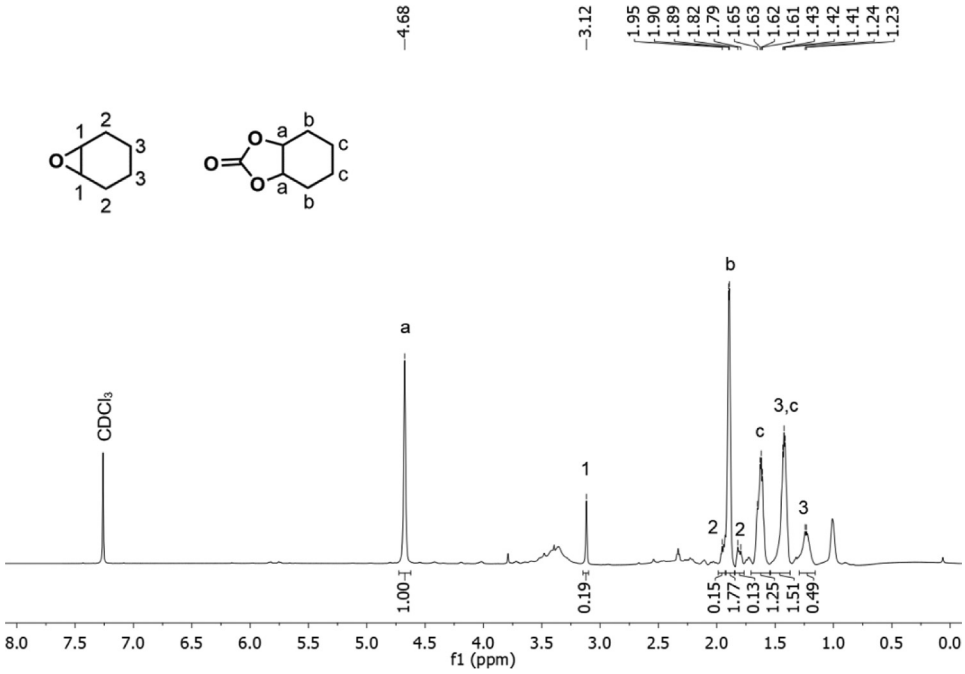

Fig. 47. ^{1}H-NMR spectrum of the cycloaddition of CO_2 to epoxy cyclohexane using 2 mol% **$SnCl_4$(0.66)-IL-Br** at 100°C, 15 bar CO_2 for 48 h.

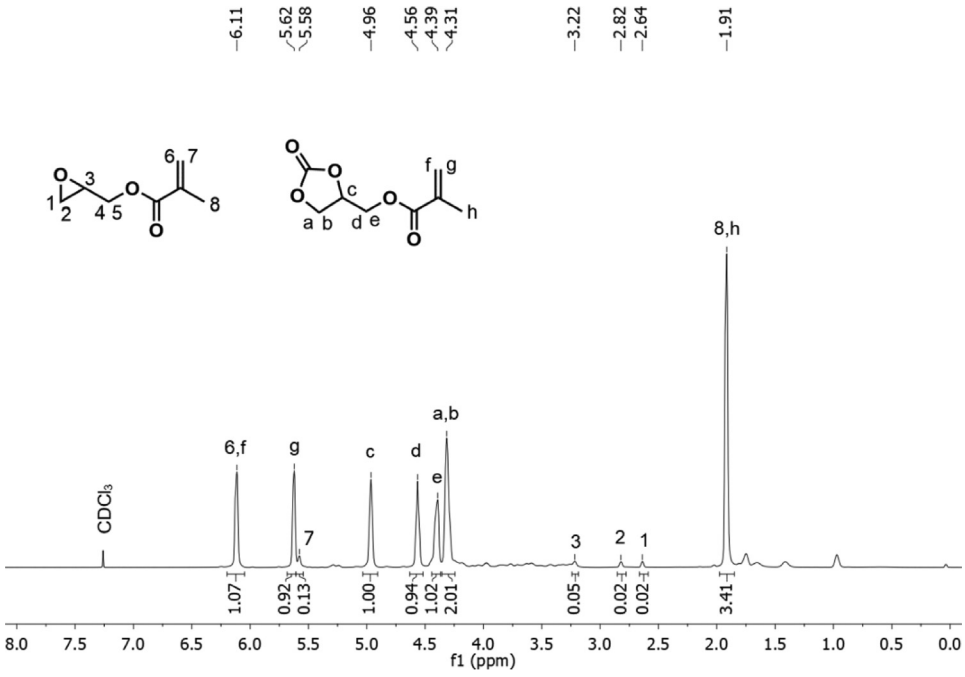

Fig. 48. ^{1}H-NMR spectrum of the cycloaddition of CO_2 to glycidyl methacrylate using 2 mol% **$ZnCl_2$(1.99)-IL-I** at 40°C, 1 bar 50% CO_2 in N_2 for 24 h.

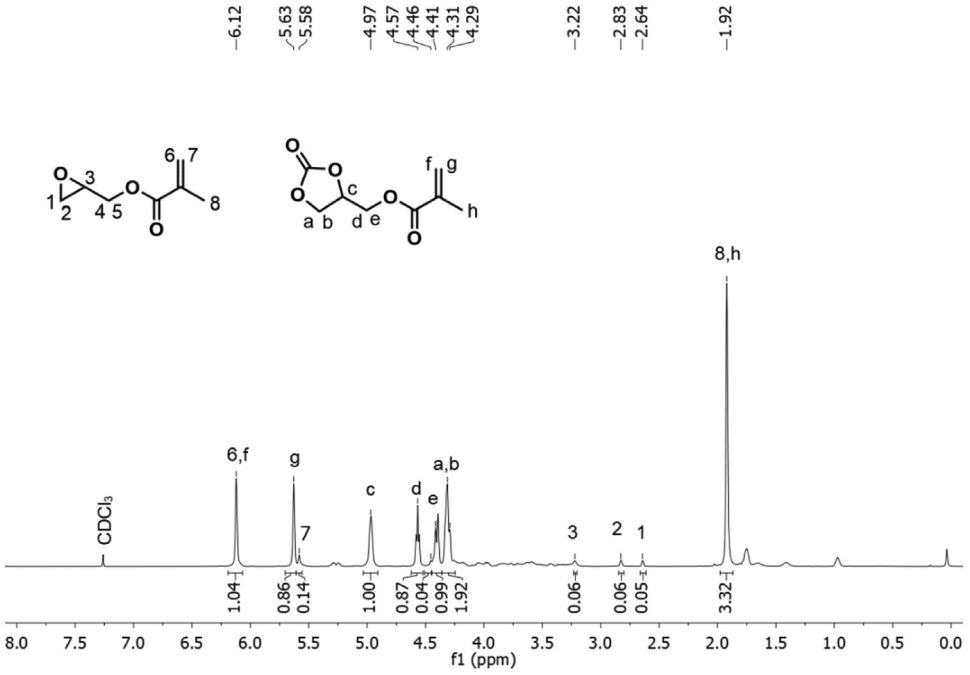

Fig. 49. ^{1}H-NMR spectrum of the cycloaddition of CO_2 to glycidyl methacrylate using 2 mol% **$SnCl_4$(0.66)-IL-Br** at 40°C, 1 bar 50% CO_2 in N_2 for 24 h.

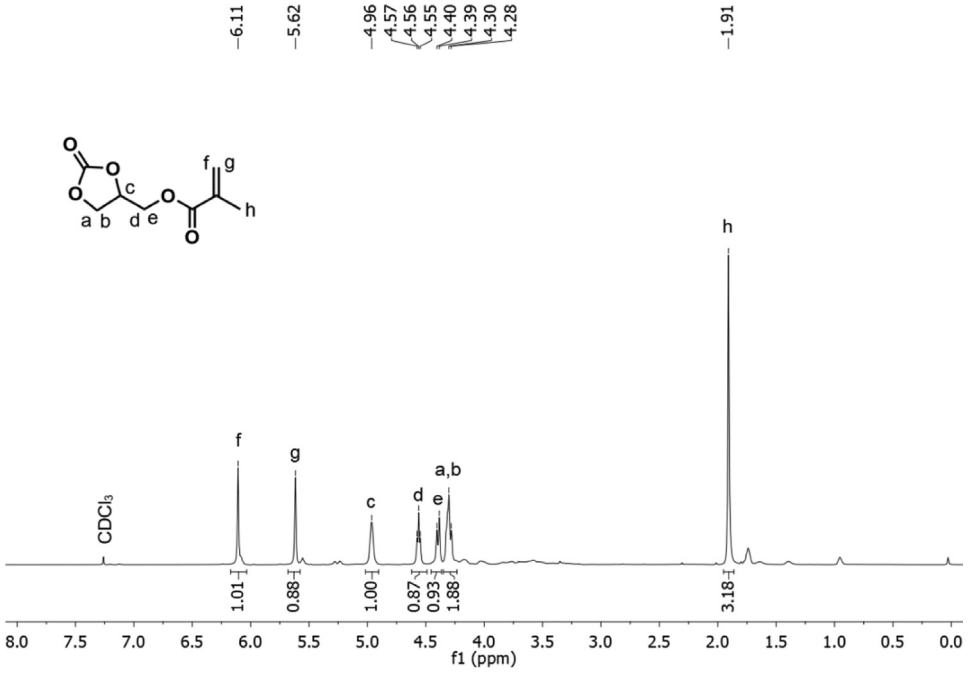

Fig. 50. ^{1}H-NMR spectrum of the cycloaddition of CO_2 to glycidyl methacrylate using 2 mol% **$ZnCl_2$(1.99)-IL-I** at 40°C, 1 bar 20% CH_4 in CO_2 for 24 h.

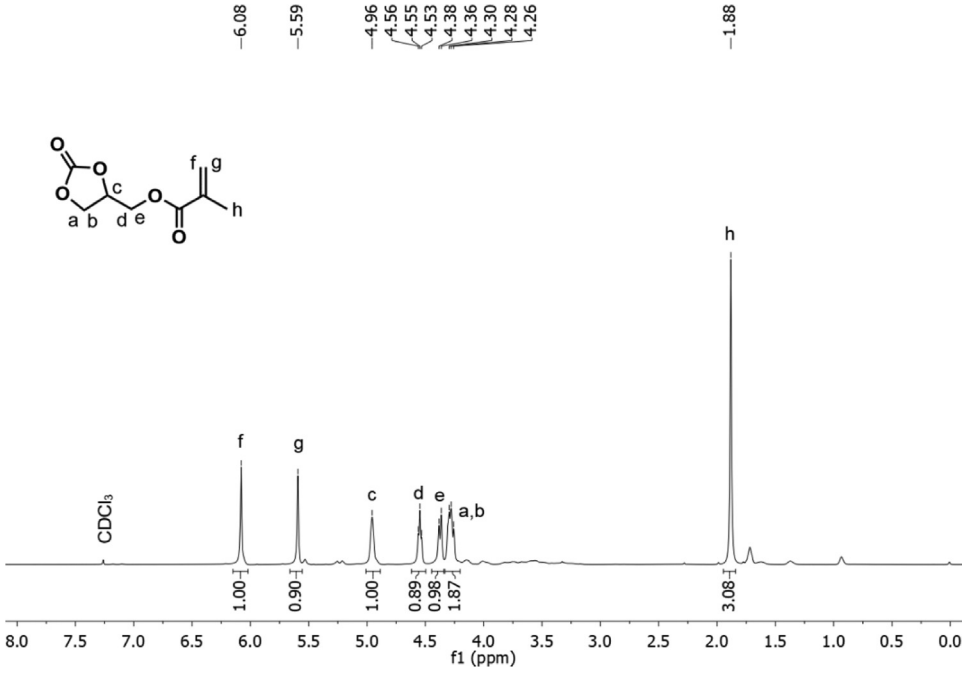

Fig. 51. ^{1}H-NMR spectrum of the cycloaddition of CO_2 to glycidyl methacrylate using 2 mol% **$SnCl_4$(0.66)-IL-Br** at 40°C, 1 bar 20% CH_4 in CO_2 for 24 h.

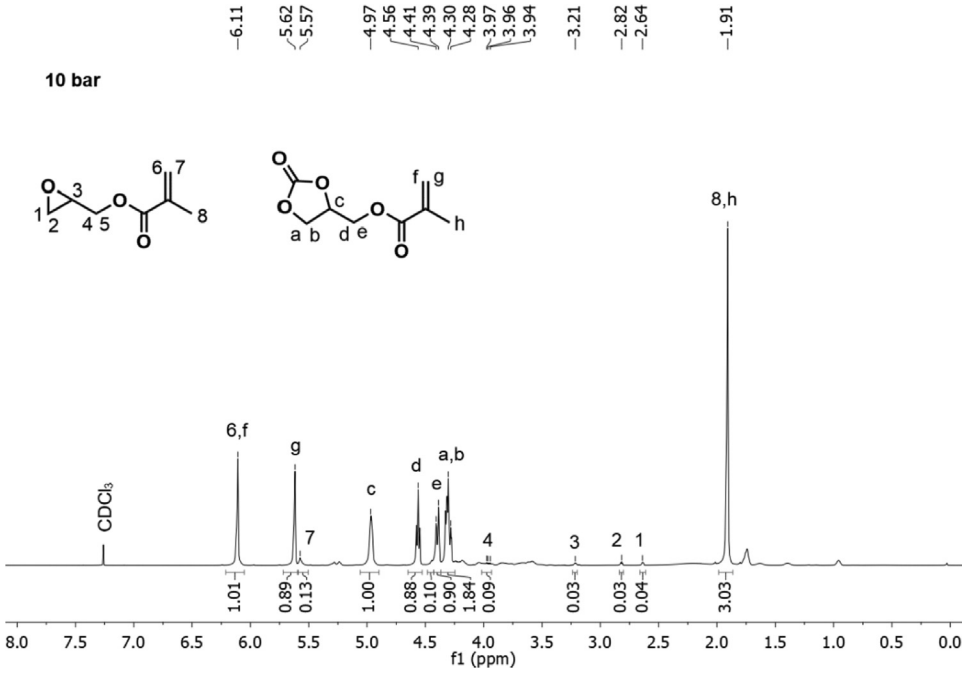

Fig. 52. ^{1}H-NMR spectrum of the cycloaddition of CO_2 to glycidyl methacrylate using 1 mol% **$ZnCl_2$(1.99)-IL-I** at 100°C, 10 bar CO_2 for 1 h.

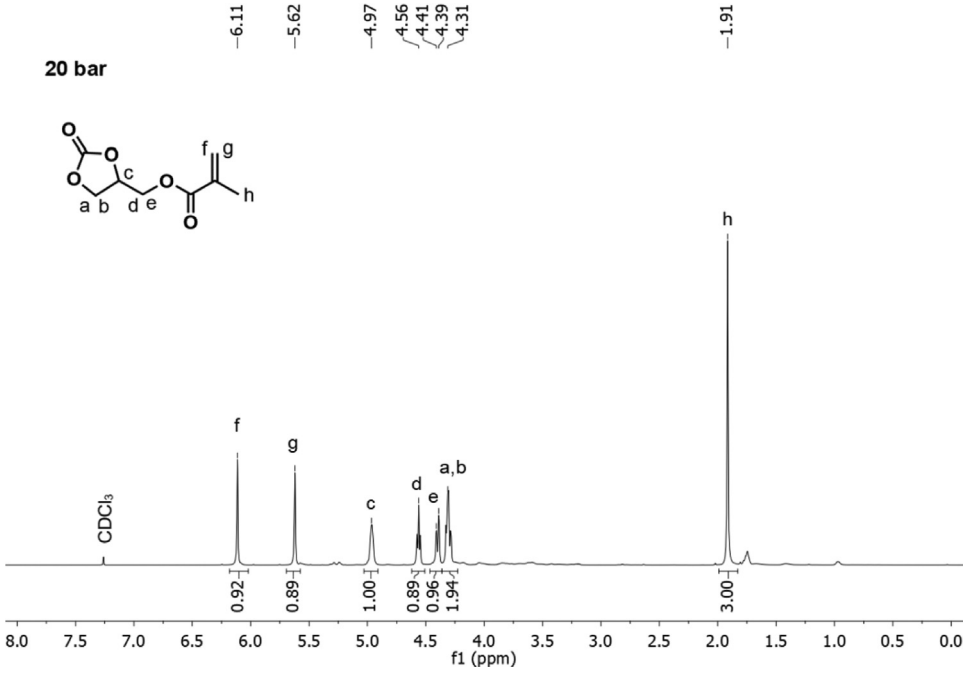

Fig. 53. ^{1}H-NMR spectrum of the cycloaddition of CO_2 to glycidyl methacrylate using 1 mol% **$ZnCl_2$(1.99)-IL-I** at 100°C, 20 bar CO_2 for 1 h.

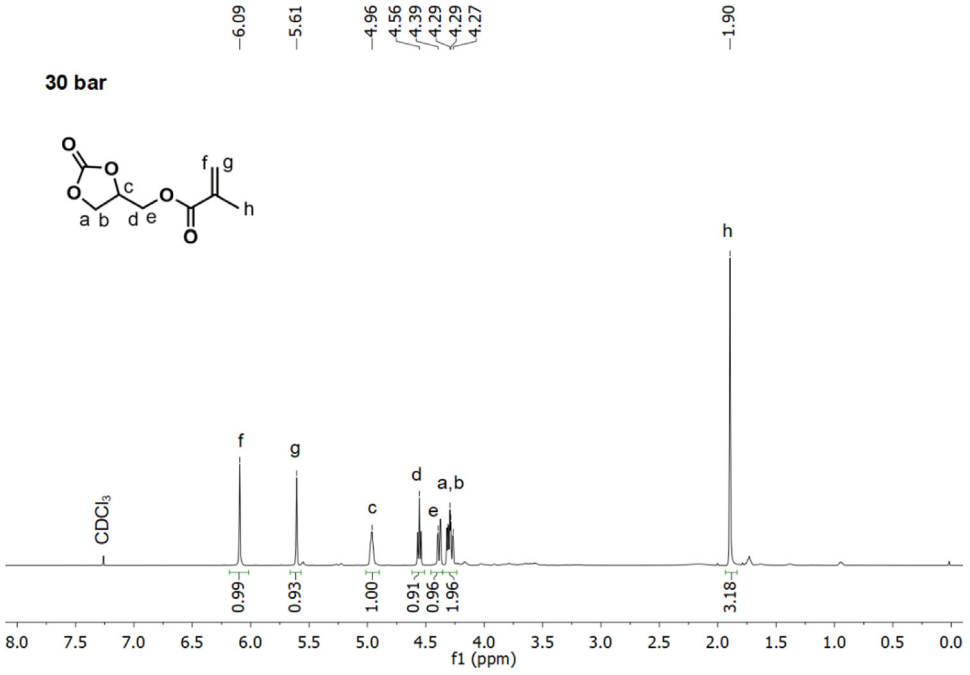

Fig. 54. ^{1}H-NMR spectrum of the cycloaddition of CO_2 to glycidyl methacrylate using 1 mol% **$ZnCl_2$(1.99)-IL-I** at 100°C, 30 bar CO_2 for 1 h.

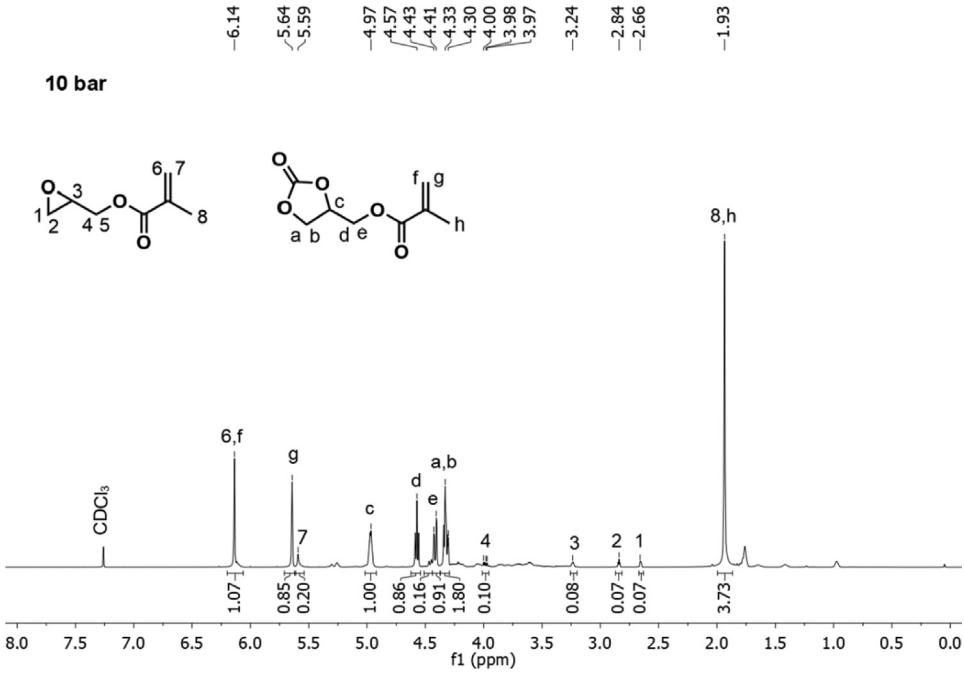

Fig. 55. ^{1}H-NMR spectrum of the cycloaddition of CO_2 to glycidyl methacrylate using 1 mol% **$SnCl_4$(0.66)-IL-Br** at 100°C, 10 bar CO_2 for 1 h.

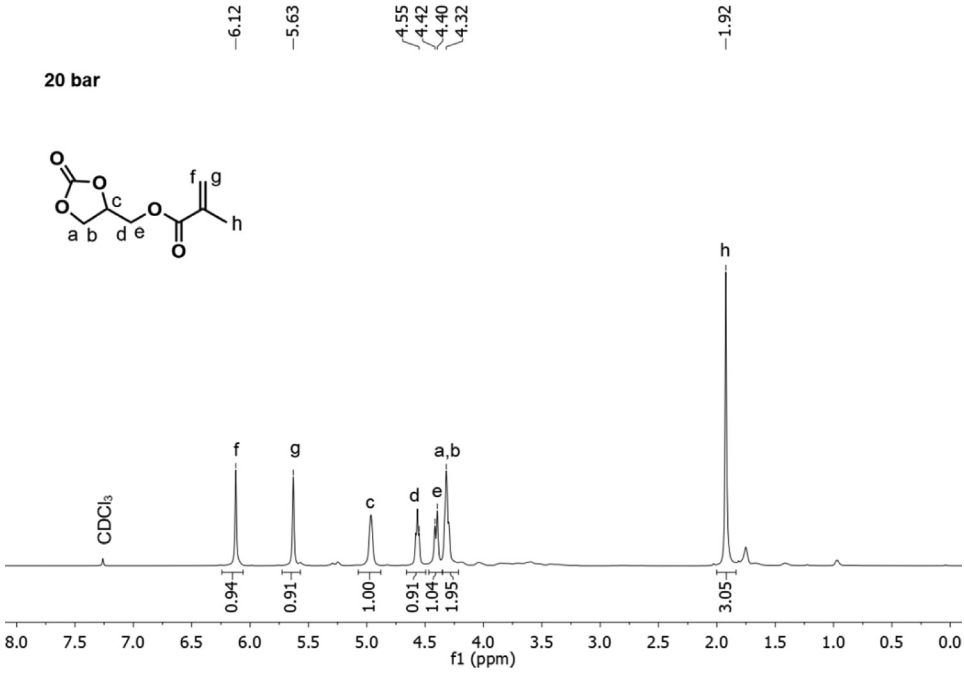

Fig. 56. ^{1}H-NMR spectrum of the cycloaddition of CO_2 to glycidyl methacrylate using 1 mol% **$SnCl_4$(0.66)-IL-Br** at 100°C, 20 bar CO_2 for 1 h.

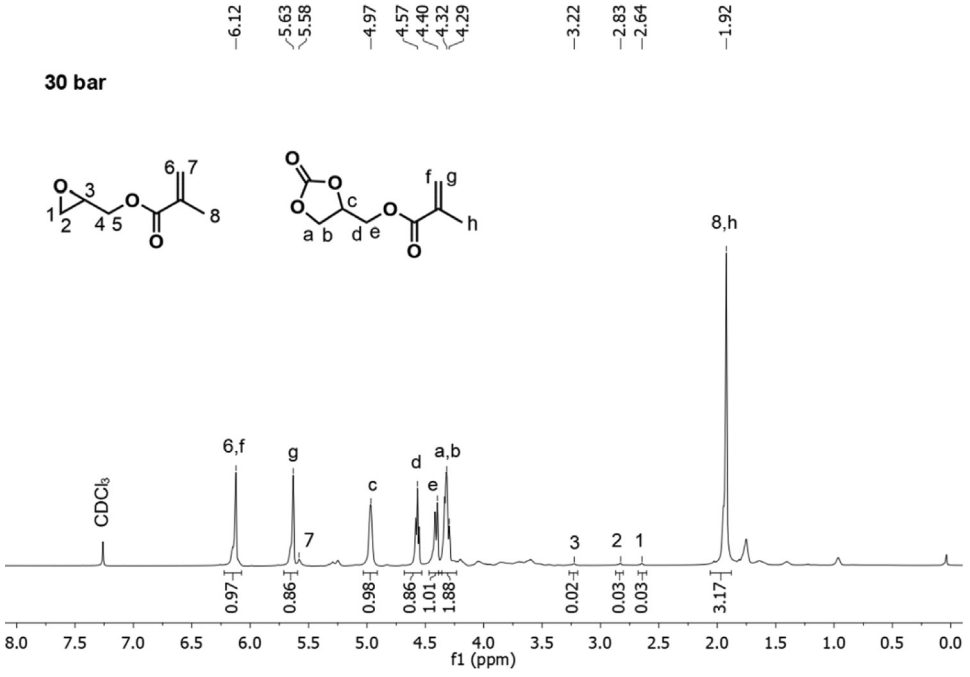

Fig. 57. ^{1}H-NMR spectrum of the cycloaddition of CO_2 to glycidyl methacrylate using 1 mol% **$SnCl_4$(0.66)-IL-Br** at 100°C, 30 bar CO_2 for 1 h.

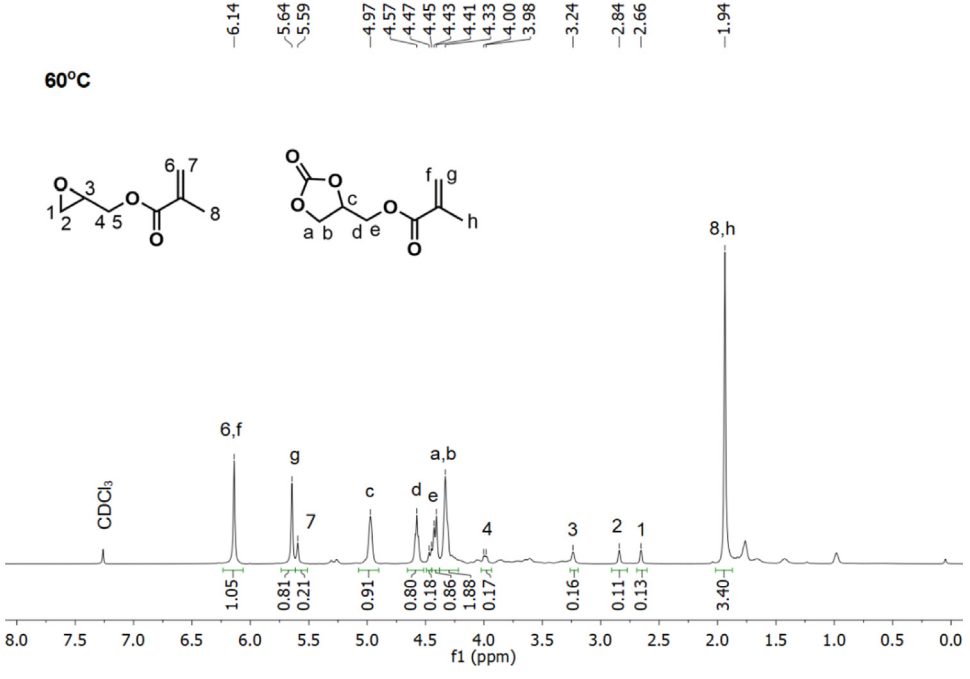

Fig. 58. ^{1}H-NMR spectrum of the cycloaddition of CO_2 to glycidyl methacrylate using 2 mol% **$ZnCl_2$(1.99)-IL-I** at 60°C, 10 bar CO_2 for 1 h.

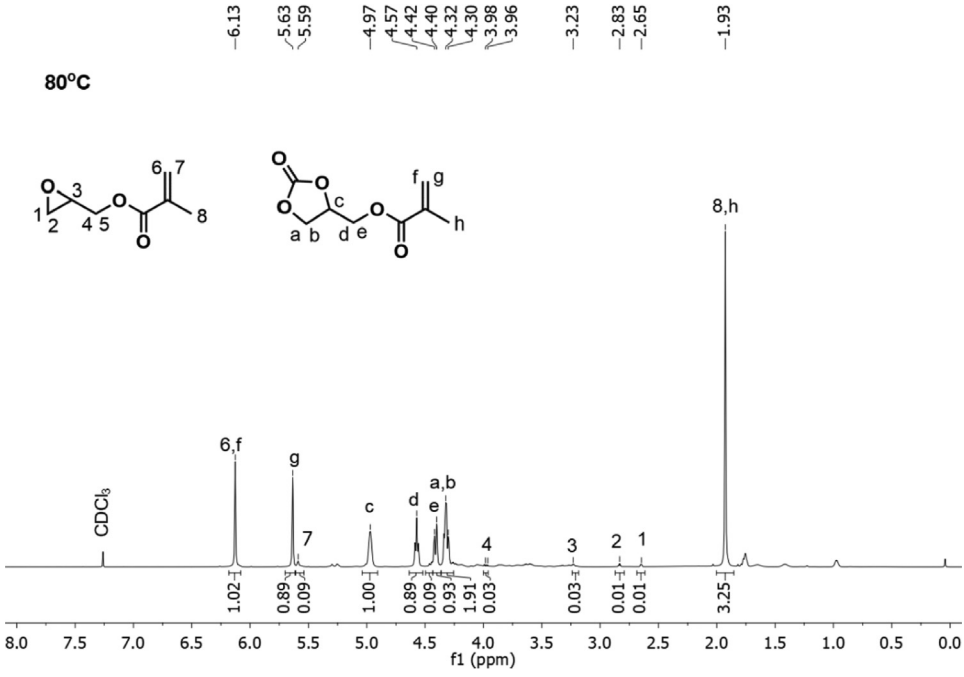

Fig. 59. ^{1}H-NMR spectrum of the cycloaddition of CO_2 to glycidyl methacrylate using 2 mol% **$ZnCl_2$(1.99)-IL-I** at 80°C, 10 bar CO_2 for 1 h.

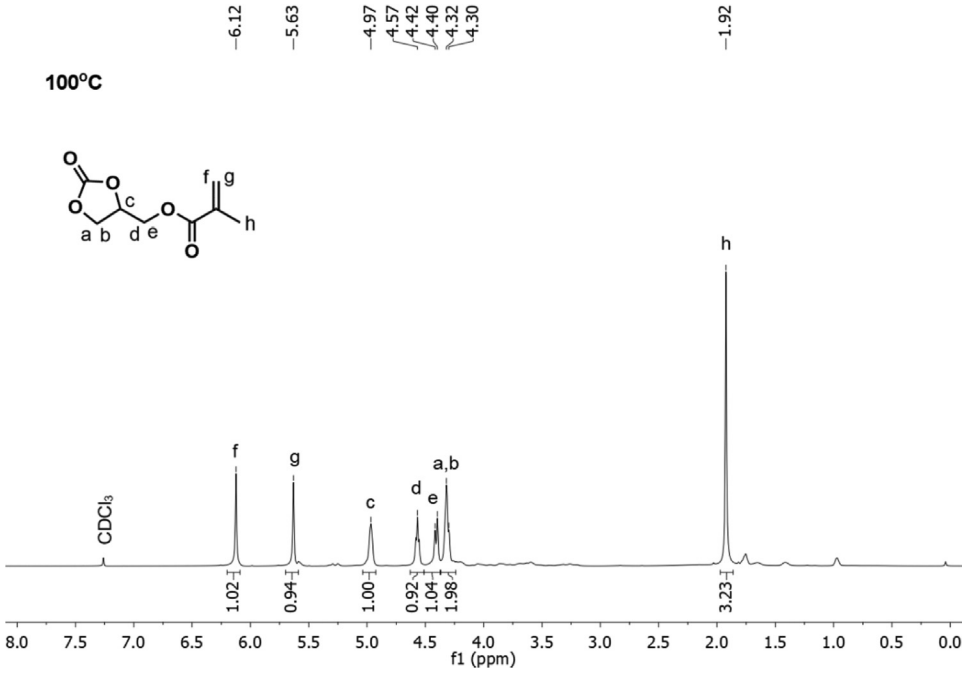

Fig. 60. ^{1}H-NMR spectrum of the cycloaddition of CO_2 to glycidyl methacrylate using 2 mol% **$ZnCl_2$(1.99)-IL-I** at 100°C, 10 bar CO_2 for 1 h.

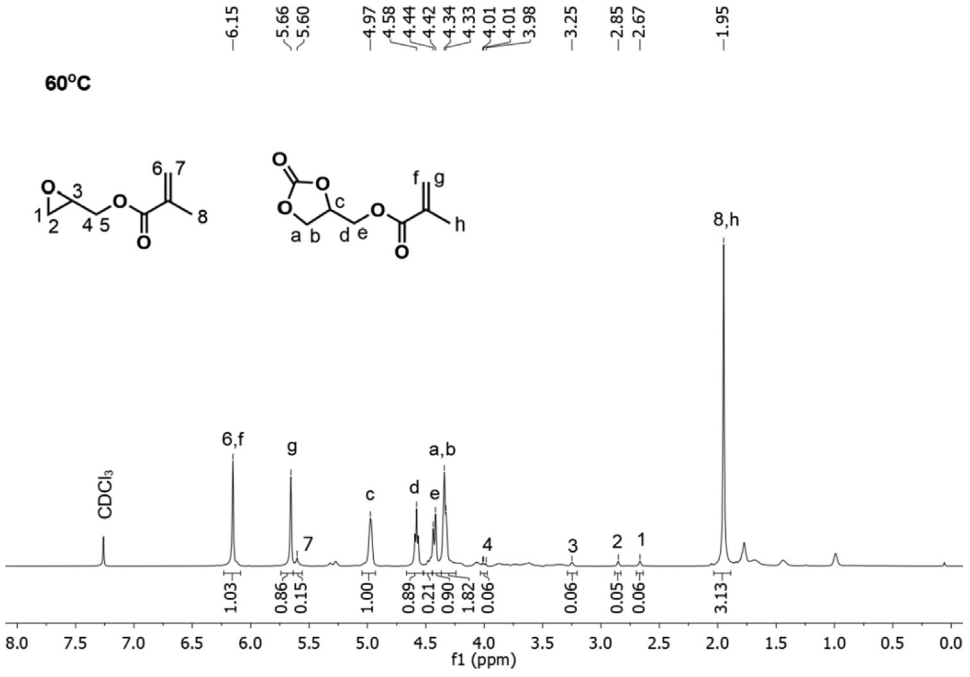

Fig. 61. ^{1}H-NMR spectrum of the cycloaddition of CO_2 to glycidyl methacrylate using 2 mol% **$SnCl_4$(0.66)-IL-Br** at 60°C, 10 bar CO_2 for 1 h.

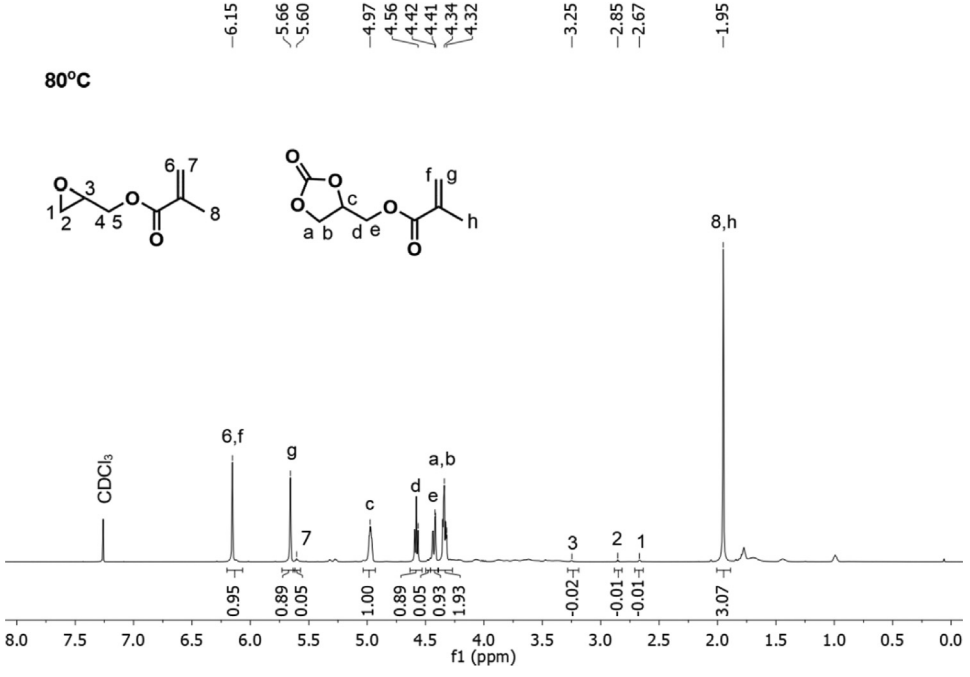

Fig. 62. ^{1}H-NMR spectrum of the cycloaddition of CO_2 to glycidyl methacrylate using 2 mol% **$SnCl_4$(0.66)-IL-Br** at 80°C, 10 bar CO_2 for 1 h.

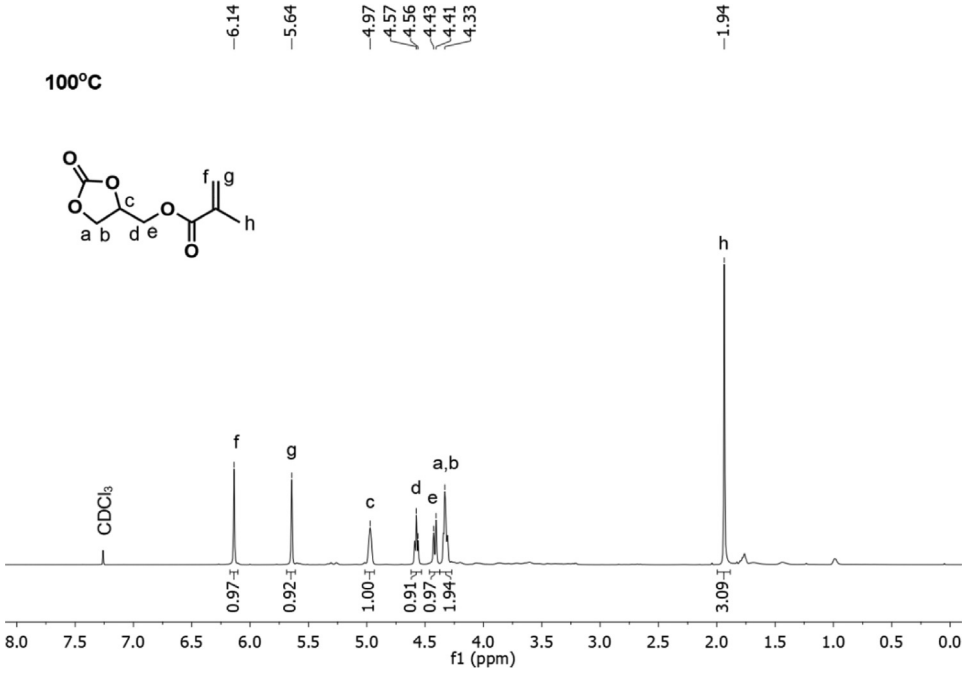

Fig. 63. ^{1}H-NMR spectrum of the cycloaddition of CO_2 to glycidyl methacrylate using 2 mol% **$SnCl_4$(0.66)-IL-Br** at 100°C, 10 bar CO_2 for 1 h.

CRediT Author Statement

Chalida Phungpanya: Investigation, data curation; **Ounjit Sodpiban:** Data curation, Investigation, Writing - Original draft preparation; **Silvano Del Gobbo:** Visualization, Investigation, Data curation; **Sunatda Arayachukiat:** Validation, Data curation; **Taradon Pimochart:** Validation, Supervision; **Valerio D' Elia:** Supervision, data curation, Writing - reviewing & editing.

Declaration of Competing Interest

The authors declare that they have no known competing financial interests or personal relationships which have or could be perceived to have influenced the work reported in this article.

Acknowledgments

C.P and S.D.G. would like to acknowledge financial support through postdoctoral fellowship from the Vidyasirimedhi Institute of Science and Technology, V.D.E. thanks the Thailand Research Fund (Grant No. RSA6080059) for funding this research.

Supplementary Materials

Supplementary material associated with this article can be found in the online version at doi:10.1016/j.dib.2021.107190.

References

[1] F.Della Monica, A.W. Kleij, Mechanistic guidelines in nonreductive conversion of CO2: the case of cyclic carbonates, Catal. Sci. Technol. 10 (2020) 3483–3501, doi:10.1039/D0CY00544D.
[2] H. Büttner, L. Longwitz, J. Steinbauer, C. Wulf, T. Werner, Recent developments in the synthesis of cyclic carbonates from epoxides and CO2, Top. Curr. Chem. (2017) 375, doi:10.1007/s41061-017-0136-5.
[3] J.W. Comerford, I.D.V. Ingram, M. North, X. Wu, Sustainable metal-based catalysts for the synthesis of cyclic carbonates containing five-membered rings, Green Chem 17 (2015) 1966–1987, doi:10.1039/C4GC01719F.
[4] M. Alves, B. Grignard, R. Mereau, C. Jerome, T. Tassaing, C. Detrembleur, Organocatalyzed coupling of carbon dioxide with epoxides for the synthesis of cyclic carbonates: catalyst design and mechanistic studies, Catal. Sci. Technol. 7 (2017) 2651–2684, doi:10.1039/C7CY00438A.
[5] X. Jin, J. Ding, Q. Xia, G. Zhang, C. Yang, J. Shen, B. Subramaniam, R.V. Chaudhari, Catalytic conversion of CO2 and shale gas-derived substrates into saturated carbonates and derivatives: Catalyst design, performances and reaction mechanism, J. CO2 Util. 34 (2019) 115–148, doi:10.1016/j.jcou.2019.05.024.
[6] O. Sodpiban, C. Phungpanya, S. Del Gobbo, S. Arayachukiat, T. Piromchart, V. D'Elia, Rational engineering of single-component heterogeneous catalysts based on abundant metal centers for the mild conversion of pure and impure CO_2 to cyclic carbonates, Chem. Eng. J. 422 (2021) 129930, doi:10.1016/j.cej.2021.129930.
[7] N. Yadav, F. Seidi, S. Del Gobbo, V. D'Elia, D. Crespy, Versatile functionalization of polymer nanoparticles with carbonate groups via hydroxyurethane linkages, Polym. Chem. 10 (2019) 3571–3584, doi:10.1039/c9py00597h.
[8] C.J. Whiteoak, A. Nova, F. Maseras, A.W. Kleij, Merging sustainability with organocatalysis in the formation of organic carbonates by using CO2 as a feedstock, ChemSusChem 5 (2012) 2032–2038, doi:10.1002/cssc.201200255.
[9] O. Sodpiban, S. Del Gobbo, S. Barman, V. Aomchad, P. Kidkhunthod, S. Ould-Chikh, A. Poater, V. D'Elia, J.-M. Basset, Synthesis of well-defined yttrium-based Lewis acids by capturing a reaction intermediate and catalytic application for cycloaddition of CO2 to epoxides under atmospheric pressure, Catal. Sci. Technol. 9 (2019) 6152–6165, doi:10.1039/c9cy01642b.
[10] G. Chen, Y. Zhang, J. Xu, X. Liu, K. Liu, M. Tong, Z. Long, Imidazolium-based ionic porous hybrid polymers with POSS-derived silanols for efficient heterogeneous catalytic CO2 conversion under mild conditions, Chem. Eng. J. 381 (2020) 122765, doi:10.1016/j.cej.2019.122765.
[11] W. Natongchai, S. Pornpraprom, V. D'Elia, Synthesis of bio-based cyclic carbonates using a bio-based hydrogen bond donor: application of ascorbic acid to the cycloaddition of CO2 to oleochemicals, Asian J. Org. Chem. 9 (2020) 801–810, doi:10.1002/ajoc.202000154.
[12] S. Arayachukiat, P. Yingcharoen, S.V.C. Vummaleti, L. Cavallo, A. Poater, V. D'Elia, Cycloaddition of CO_2 to challenging N-tosyl aziridines using a halogen-free niobium complex: catalytic activity and mechanistic insights, Mol. Catal. 443 (2017) 280–285, doi:10.1016/j.mcat.2017.10.023.